Energetics of Metal Oxide Solid Solutions

Jeremy K. Burdett* and Chinh Nguyen

Department of Chemistry and James Franck Institute, The University of Chicago, Chicago, Illinois 60637

Received August 5, 1993. Revised Manuscript Received September 21, 1993®

Excess energies of metal oxide solid solution formation have been calculated *via* tight-binding calculations on a set of 27 rock-salt-based superstructures. From these values three important factors which control the energetics of solid solutions have been identified: (i) a two-atom term, which may be identified with the volume change of solution formation; (ii) a three-atom term, which may be identified with the bulk of the metallic substitution process and understandable in terms of the regular solution model, and (iii) an asymmetry term, which is interpreted as arising *via* the interruption of a delocalized orbital network and is probably largely a four-atom term. The electron count dependence of the three terms and electronic insights provided *via* the method of moments enables an understanding of the reversal in the sign of $\Delta H_{xs}(x)$ found experimentally on going from (Fe,Mg)O to (Ni,Mg)O.

Introduction

The details of the energetics behind solid solutions of metal oxides are an important facet of the behavior of solids, influencing phase formation both under extreme geophysical conditions in the earth's mantle and under less extreme conditions in the laboratory. It is probably true to say that other than size considerations all current quantitative models are almost entirely empirical with virtually no gulding principles from theory.[1a,b] This is a state of affairs very different from that for metal alloys, where considerable theoretical insight exists.[1c] It is the purpose of this paper to calculate the heats of mixing for a series of oxide systems and to decompose the results in a way which will clearly show their origin.

A useful parameter, which determines many of the details of solid solutions, and which may often be determined experimentally, is the excess enthalpy of formation. This is given by eq 1 for a simple oxide $A_xB_{1-x}O$, where A,

$$\Delta H_{xs}(x) = \Delta H_{meas}(x) - x(\Delta H_{meas}(1) - \Delta H_{meas}(0)) \quad (1)$$

B are metal ions, and is simply the deviation in the measured enthalpy of formation, $\Delta H_{meas}(x)$ from ideality, or the deviation of the solid solution from Raoultian behavior expected by interpolation of the heats of formation of the end-members, $x = 0, 1$. 1–4 show types of

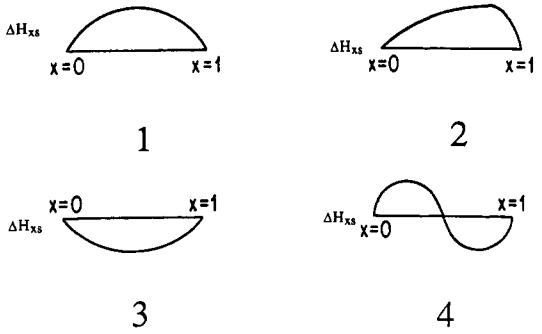

behavior which have been observed experimentally. 1 shows the very common case where $\Delta H_{xs}(x)$ is positive. Such a situation is found for example[2–6] in the (M,Mg)O systems where M = Mn, Fe, Co. The symmetric behavior about $x = 0.5$ is mimicked by the regular solution model of eq 2. X_1 and X_2 are the mole fraction of components

$$\Delta H_{xs}(x) = WX_1X_2 = Wx(1-x) \quad (2)$$

1 and 2 respectively, and W, which measures the size of the deviation, may be expressed in terms of the interaction parameters ϕ_{ij} between the atoms A and B:

$$W = 2\phi_{AB} - \phi_{AA} - \phi_{BB} \quad (3)$$

These are actually "effective parameters" between the ions, since the ions themselves lie in a matrix of oxide. The sign of W is simply determined by the relative magnitudes of these microscopic parameters. If W is large and positive, then the range of the solid solution may be limited to either large or small x, phase separation occurring where the energetic penalty for solution is large. 2 shows the asymmetric situation which has to be described by a subregular model equation (4). 3 shows the situation which

$$\Delta H_{xs}(x) = X_1X_2[AX_2 + BX_1] = (1-x)(x)[Ax + B(1-x)] \quad (4)$$

is not very common in these oxide solid solutions, where the excess enthalpy is negative. This is found, for example,[7] in the (Ni,Mg)O system which we will discuss later. 4 shows the case, sometimes found in studies of liquid solutions, and very rarely in studies of solid oxides, where oscillating behavior is found.

Complete miscibility often occurs if the end members or pure solids are similar in structural type or if the space

* Abstract published in *Advance ACS Abstracts*, November 15, 1993.

(1) (a) *Reviews in Mineralogy*; Vol 17; Carmichael, I. S. E., Eugster H. P., Eds.; *Thermodynamic Modelling of Geological Materials, Minerals, Fluids and Melts.* (b) *Reviews in Mineralogy*; Vol 14; Kieffer, S. W., Navrotsky, A., Eds.; *Microscopic to Macroscopic; Atomic Environments to Mineral Thermodynamics*, **1987**, *17*, 42. (c) Hafner, J. *From Hamiltonians to Phase Diagrams*; Springer-Verlag: New York, 1987.
(2) Hahn, Jr., W. C.; Muan, A. *Trans. AIME* **1962**, *224*, 416.
(3) Bonczar, L. C.; Graham, E. K. *J. Geophys. Res.* **1982**, *87*, 1061.
(4) Hazen, R. M.; Jeanloz, R. *Rev. Geophys. Space Phys.* **1984**, *22*, 37.
(5) Bergstein, A. *Czech. J. Phys. B* **1973**, *23*, 1141.
(6) Doman, R. C.; Barr, J. B.; McNally, R. N.; Alper, A. M. *J. Am. Ceram. Soc.* **1964**, *46*, 63, 313.
(7) Davies, P. K.; Navrotsky, A. *J. Solid State Chem.* **1981**, *38*, 264.

0897-4756/93/2805-1775$04.00/0

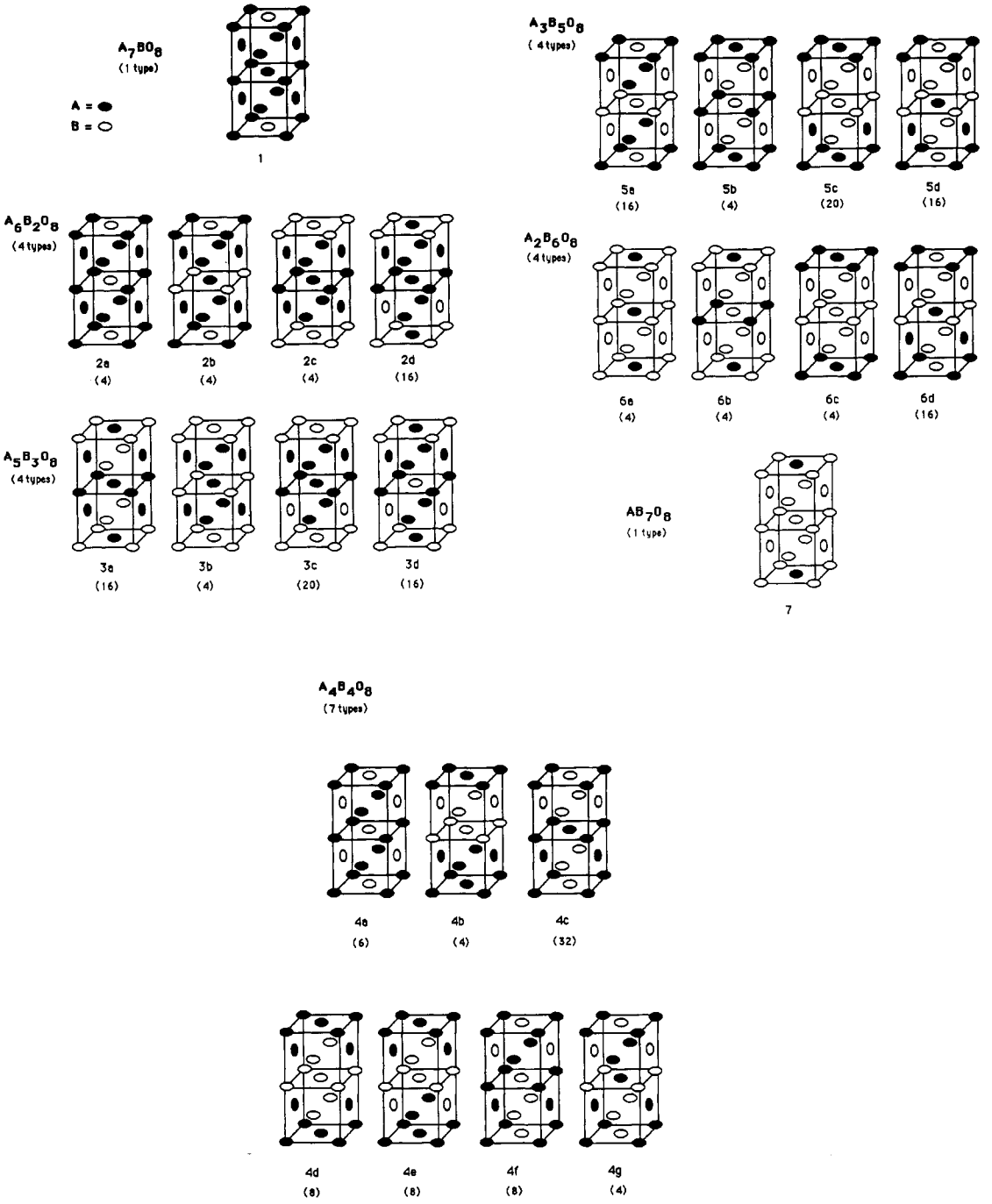

Figure 1. The 27 $A_{8-y}B_yO_8$ solid solutions. Only 25 solutions are illustrated here: the end members A_8O_8 and B_8O_8 are pure AO and BO and are not shown. In all 25 solutions or arrangements, only the metals A and B are displayed. In showing how we permute A's and B's, the face-centered cubic distribution of oxygens, for simplicity, are left out. Underneath each solution are the name and, in parentheses, the frequency of occurrence of that solution. For A_7BO_8 and AB_7O_8, there is only one possible arrangement.

group of one structure is a subgroup of the other. In classical terms using billiard ball-type models the "size" mismatch of the two components are important. Such ideas are well-developed for solid (and liquid) solutions of the simple metals.[1c] Insertion of a large ion in place of a small one or putting a small ion on the site vacated by a large one clearly lead to an energetically unfavorable situation and hence a positive $\Delta H_{xs}(x)$. Navrotsky found an approximately linear dependence for W on δ^2 in several rock-salt oxide systems,[8] where δ is defined as in eq 5 in

$$\delta = (a_1 - a_2)/(a_1 + a_2) \tag{5}$$

terms of a_i, the lattice parameter for the two components 1 and 2. A similar size difference parameter was used earlier by Kleppa[9] in the modeling of fused-salt systems.

Urusov[10] found that when the electronegativity difference between the components to be mixed is small, then eq 5 holds well for the ΔH_{xs} expression:

$$\Delta H_{xs}(x) = c(1-x)(x)nZ^2\eta^2 \tag{6}$$

(8) Navrotsky, A. In *M.T.P. Int. Rev. Sci., Inorg. Chem., Ser. 2* **1974**, *5*, 29.

(9) Kleppa, O. J. *Annu. Rev. Phys. Chem.* **1965**, *16*, 187.
(10) Urusov, V. S. *Geokhimiia*, **1970**, *4*, 510; **1968** *9*, 1033.

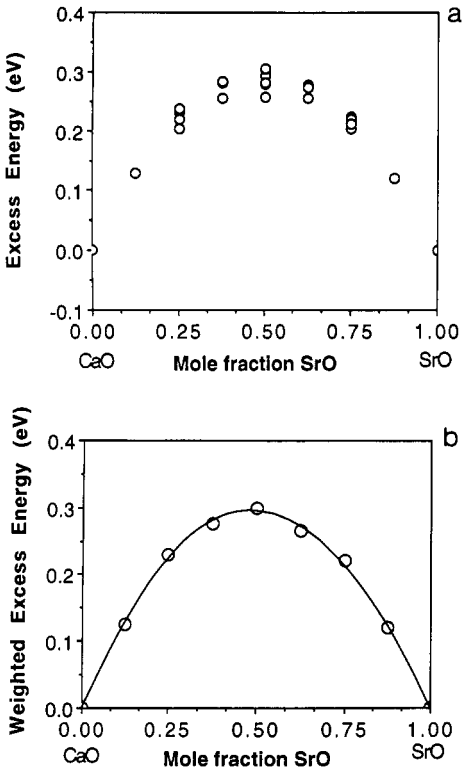

Figure 2. Computed excess energies for (Ca,Sr)O solid solutions. (a) Excess energy for each (Ca,Sr)O solid solution. (b) Weighted excess energies for (Ca,Sr)O solid solutions. Calculations used the extended Hückel Implementation of tight-binding theory.

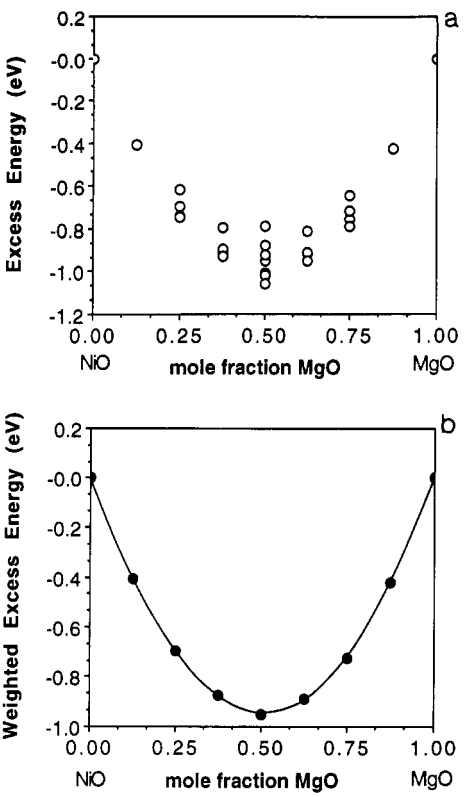

Figure 3. Computed excess energies for (Ni,Mg)O solid solutions. (a) Excess energy for each (Ni,Mg)O solid solution. (b) Weighted excess energies for (Ni,Mg)O solid solutions. Calculations used the extended Hückel Implementation of tight-binding theory.

with

$$\eta = [(V_2)^{1/3} - (V_1)^{1/3}]/[X_1(V_1)^{1/3} + X_2(V_2)^{1/3}] \quad (7)$$

Here c is an empirical parameter, n is the coordination number, Z is the charge, and V_1 and V_2 are the volumes of the two components. The importance of volume change rather than the ionic size mismatch *per se* is illustrated by the following pair of examples. Solubility is limited for (Ba,Ca)O solid solutions where the volume difference is a large percentage of the total volume, but in $(Ba_2,Ca)_2SiO_4$ complete miscibility occurs because the volume difference is a smaller percentage of the total volume and $\Delta H_{xs}(x)$ is smaller. Navrotsky and Davies[11] used W (or A or B) = $m(\Delta V) + b$, where m and b are constants and where the volume-mismatch term $\Delta V = (V_2 - V_1)/(V)$, where $V = V_1$, V_2 or their mean as appropriate. The correlation between W (or A or B) and ΔV is found to be independent of whether the ions being mixed are anions or cations and of the structure type (e.g., NaCl or CsCl). The fact that both the garnets, with the metal in eight coordination, and the rock-salt systems, with six-coordinate metals, show similar correlations suggests that coordination number is not a dominant factor. However, even this simple model has some problems. The size of the intercept (b) shows substantial and unpredictable variations from one system to another.

This size difference between host and guest ions has been considered to be the most influential factor in most theoretical models of binary solid solutions.[12-20] Using the single substitutional defect model of Dick and Das[12] that allows for local relaxation by a controlled displacement of an ion within a specific site, Fancher and Barsch[13] found that a smaller guest ion can be placed on the site of a larger host ion with a smaller energetic penalty than the converse where a larger ion is squeezed into a smaller site. For example, a 1% substitution of K for Na in KBr is calculated to have a lower heat of formation (141 J/mol) than a similar substitution of K for Na in NaBr (194 J/mol). A related example of the effect of the size difference is also found in the asymmetric solvus of $(K,Na)AlSi_3O_8$, an alkali feldspar.[14]

In addition to the relative size of the components, the stability of solid solutions has been suggested to depend on at least two other factors, but in a less well-determined way. They are usually invoked only when size arguments fail. These are the effects of covalency and the influence of transition-metal ions. Even when the two ions are of similar size, a large difference in covalency apparently limits the solid solubilities. Examples include (Na,Ag)Cl and (Na,Ag)Br, both of which have large values of $\Delta H_{xs}(x)$.[19] The importance of effects associated with d orbital occupancy, sometimes phrased in terms of transition-metal crystal-field stabilization energy[20] has also been recognized.

This paper will concern itself with an exploration of some of the factors behind the shape of these curves in

(11) Davies, P. K.; Navrotsky, A. *J. Solid State Chem.* **1983**, *46*, 1.
(12) Dick, B. G.; Das, T. P. *Phys. Rev.* **1962**, *127*, 1053.
(13) Fancher, D. L.; Barsch, G. R. *J. Phys. Chem. Solids* **1969**, *30*, 2503.
(14) Thompson, Jr., J. B.; Waldbaum, D. R. *Am. Miner.*, **1968**, *53*, 1965.
(15) Haselton, Jr., H. T.; Westrum, E. F. *Geochim. Cosmochim. Acta* **1980**, *44*, 701.
(16) Kleppa, O. J.; Meschel, S. *J. Phys. Chem.* **1965**, *69*, 3531.
(17) Wasastjerna, J. A. *Soc. Sci. Fenn. Comment. Phys. Math.* **1948**, *14*, 5.
(18) Fancher, D. L.; Barsch, G. R. *J. Phys. Chem. Solids* **1969**, *30*, 2517.
(19) Fancher, D. L.; Barsch, G. R. *J. Phys. Chem. Solids* **1971**, *32*, 1303.
(20) Newton, R. C.; Wood, B. J. *Am. Miner.*, **1980**, *65*, 733.

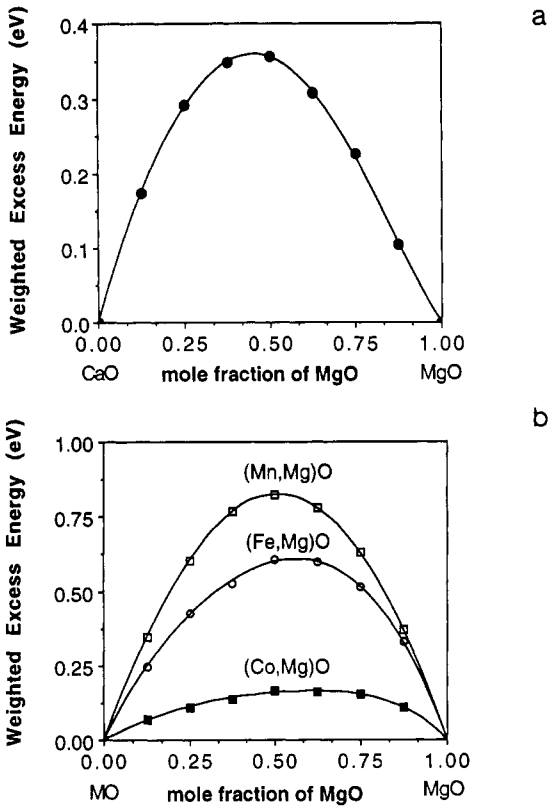

Figure 4. Computed excess energies for (M,Mg)O solid solutions where M = Ca, Mn, Fe, and Co: (a) M = Ca; (b) M = Mn, Fe, and Co.

Table I. Experimental and Calculated Values of the Interaction Parameters for Rock-Salt (M,Mg)O Solid Solutions

MO	(MO)[a] (Å)	M–O bond dist (Å)	W or A,B of (M,Mg)O expt (kJ/mol)	W or A,B of (M,Mg)O calcd (kJ/mol)
CaO	4.8105	2.4052	60.6	16.8
MnO	4.4448	2.2224	18.277	39.7
FeO	4.3057	2.1528	15.945	29.6
CoO	4.2667	2.1334	4.799	8.1
NiO[b]	4.1684	2.0842	-13.538	-45.6
			-21.971	-47.1
			-5.103	-44.1
MgO	4.2121	2.1060		

[a] Navrotsky and Davies.[11] [b] For NiO, the values of W, A, and B are respectively listed.

terms of the electronic details of the problem. Our results will be supported by a one-electron model, through calculations on both molecular clusters and infinite solids using the extended Hückel approach. As with all theoretical models there will be some caveats associated with our results which we will discuss at appropriate places in the paper. We will take advantage of a unique advantage the theorist has over the experimentalist here, in being able to analyze in detail by "computational experiment" the origin of the calculated excess enthalpies of formation.

The Model

Our investigation will be concerned with a study of the energetics of binary solutions of rock-salt-based metal oxides and metal sulfides. These systems have simple structures, and the thermodynamics of their mixing behavior have been well-studied.[2-6,7,11] We hope that the results of this study will be broadly transferable to analogous phenomena in more complex solids. To model

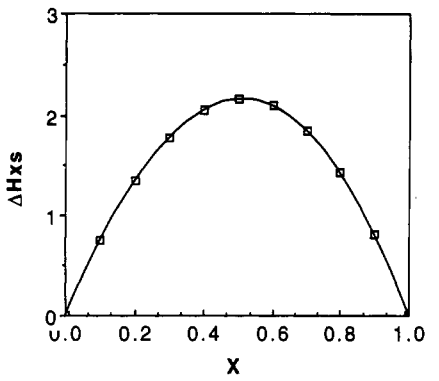

Figure 5. Excess electrostatic energy as a function of composition or mole fraction.

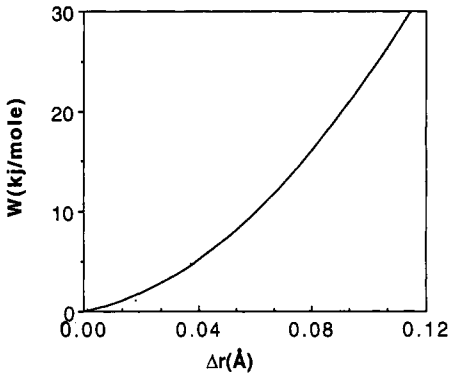

Figure 6. Dependence of W, the regular solution parameter, on Δr on the ionic model. W is in arbitrary units.

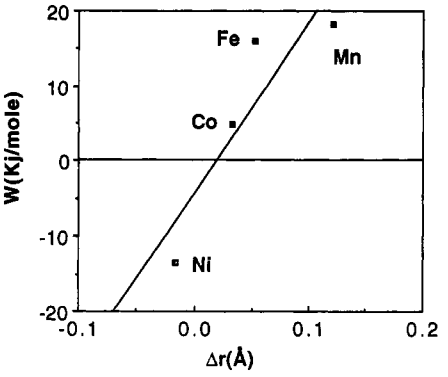

Figure 7. Experimentally determined values of W versus Δr.

a system which is by definition made up of a collection of metal atoms randomly arranged on a collection of atomic sites, we use the well-established method[21] of averaging the energies of a statistically weighted set of permutations. The model thus assumes that the solid solution contains microdomains of given stoichiometry and ordering pattern. An eight atom tetragonal unit cell $A_{8-y}B_yX_8$ (A = Mn, Fe, Co, Ni or Ca; B = Mg or Sr; X = O; and y = 0–8), represents a good compromise between the competing demands of computational economy and the generation of an appreciable number of permutations found at a specific composition or value of y. Figure 1 shows some of the 27 distinctive solid solutions found for a cell of this size. The simple rock-salt end-members, A_8X_8 and B_8X_8, are not shown. The variation of the cubic lattice parameter (a) across a solid solution range of two isostructural materials

(21) Anderson, J. S. In *Problems of Non-Stoichiometry*; Rabenau, A., Eds.; North-Holland: Amsterdam, 1970.

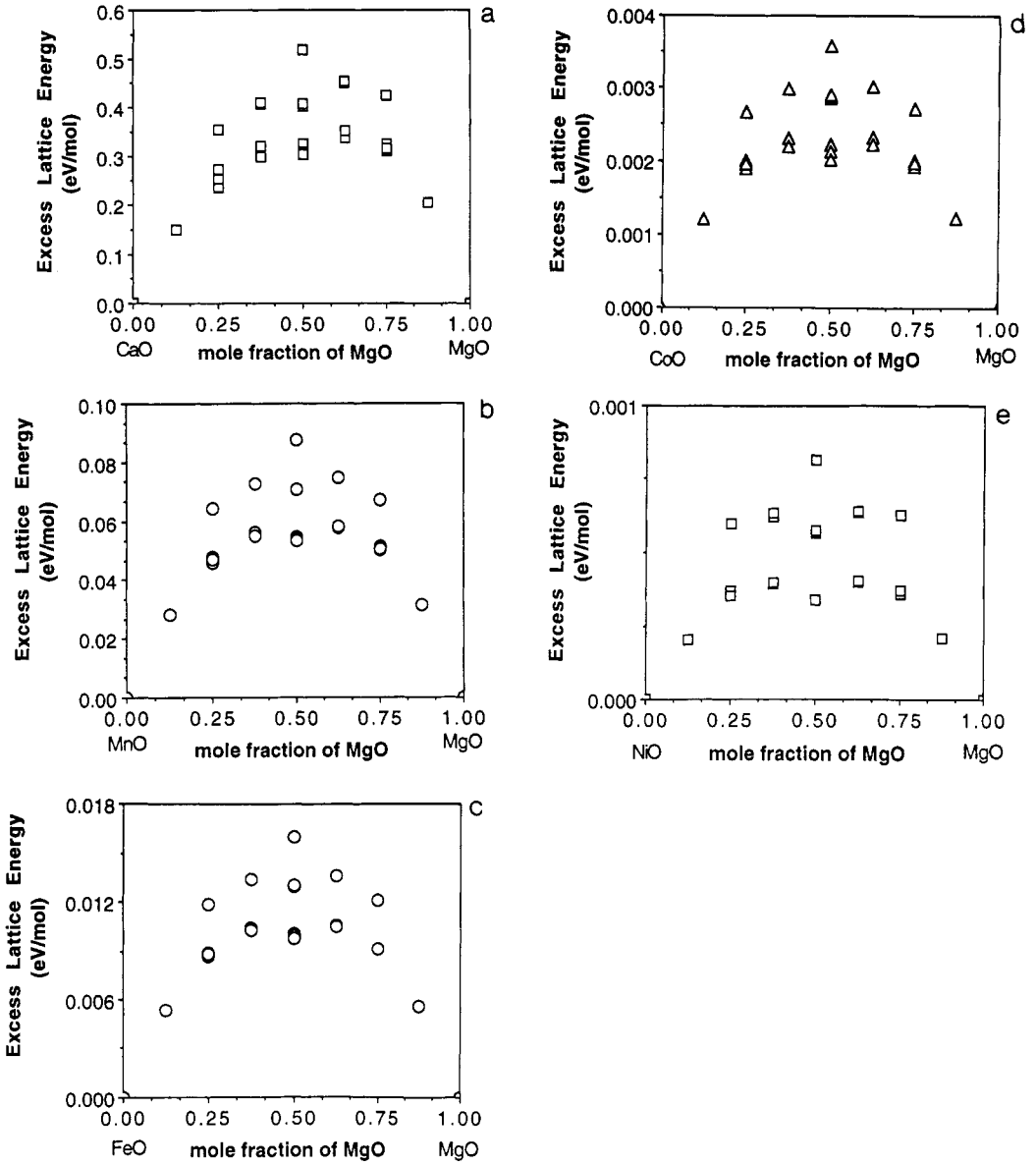

Figure 8. The 27 calculated molar excess lattice energies for (M,Mg)O: (a) M = Ca, (b) M = Mn, (c) M = Co, (d) M = Fe, and (e) M = Ni, using the interatomic potential of eq 10.

is generally assumed to be linear (Vérgard's law[17,22-24]) where $a_{solution} = (X_1a_1 + X_2a_2)$, although Zen's law[25] uses the analogous relationship in terms of the volume, $V_{solution} = (X_1V_1 + X_2V_2)$. Thus the a (and c) lattice parameters of the $A_{8-y}B_yX_8$ unit cells are just

$$a\{A_{8-y}B_yX_8\} = ((8-y)/8)a\{A_8X_8\} + (y/8)a\{B_8X_8\} \quad (8)$$

a relationship borne out experimentally for these systems. In some cases we will keep the lattice constants fixed so as to examine the energetic effect of constant-volume processes. Initially, our calculations will focus on the energetics of geometrically ideal solutions where one ion is substituted for another at a site in the crystal with no local geometrical relaxation. We ignore in our studies any problems associated with nonstoichiometry, as in wüstite FeO, for example.

Computed excess enthalpies (indicated by a') can be evaluated by analogy with eq 1 as

$$\Delta H'_{xs}\{A_{8-y}B_yX_8\} = H_{eh}\{A_{8-y}B_yX_8\} - ((8-y)/8)H_{eh}\{A_8X_8\} + (y/8)H_{eh}\{B_8X_8\} \quad (9)$$

where $H_{eh}\{A_{8-y}B_yX_8\}$ is the computed energy of a specific permutation with fixed composition evaluated via the extended Hückel implementation of the tight-binding method.[26,27] The relevant parameters are listed in Table V. We may then define $\Delta H'_{xs}(y)$ as the statistically averaged computed energies (enthalpies) of a set of permutations with composition y. The set of permutations of Figure 1 lead to seven distinct values of y ($^1/_8$ to $^7/_8$).

Figures 2 and 3 show computed values of the excess energies of the 27 permutations ($\Delta H'_{xs}\{A_{8-y}B_yX_8\}$) and the averaged energies ($\Delta H'_{xs}(y)$) which result for the (Ca, Sr)O and (Ni,Mg)O solid solutions, respectively. Figure

(22) Pearson, W. B. *The Crystal Chemistry and Physics of Metals and Alloys*; John Wiley & Sons, Inc.: New York, 1972; pp 174–194.
(23) Vegard, L. *Z. Phys.* **1921**, *5*, 17.
(24) Vegard, L.; Dale, H. *Z. Kristallogr.* **1928**, *67*, 148.
(25) Zen, E. *Am. Miner.* **1956**, *41*, 523.
(26) Hoffmann, R. *Solids and Surfaces; A Chemist's View of Bonding in Extended Structures*; VCH Publishers: New York, 1988.
(27) Burdett, J. K. *Prog. Solid State Chem.* **1984**, *15*, 173.

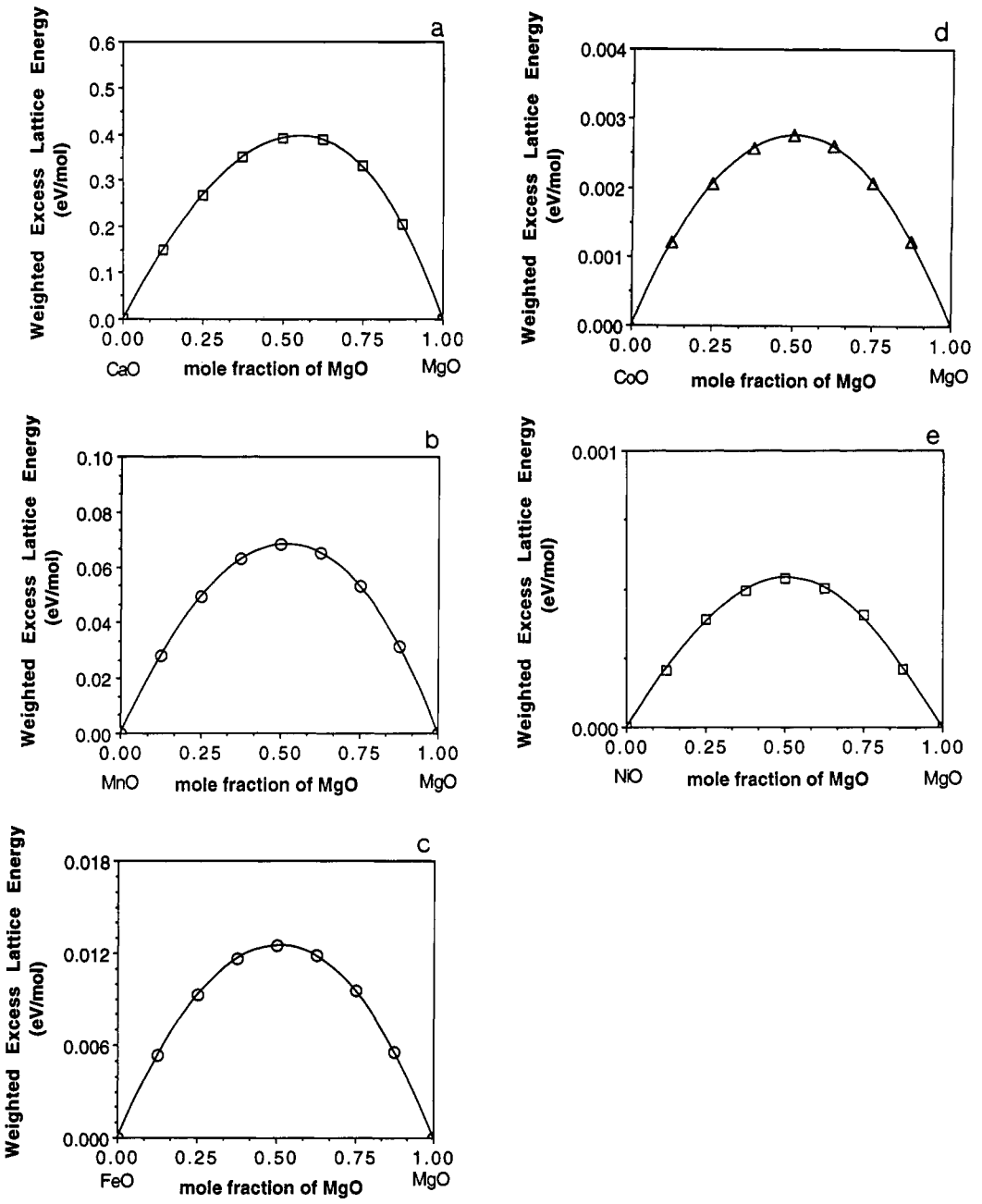

Figure 9. Weighted excess lattice energy curves for (M,Mg)O: (a) M = Ca, (b) M = Mn, (c) M = Co, (d) M = Fe, and (e) M = Ni, using the interatomic potential of eq 10.

4 shows some results for other (M,Mg) systems where M = transition metal. It is important to describe how these figures were generated. Electronically the transition-metal ions in these materials are certainly strongly localized so that the band model used here could be regarded as inappropriate. However, we do know that even within the localized wave function there is often a strong memory of the delocalized one. For example,[28] in La_2CuO_4, even though a local density calculation showed the material to be a metal described by a delocalized wave function, rather than the localized insulator which it is, many of the properties of the material were reproduced using the band model. Also we note the superexchange phenomenon[29] which allows one metal atom to "see" its neighbor in an oxide lattice *via* orbital mixing with the s and p orbitals of the connecting anion, in this case oxygen. This is true in systems of the type we study here where "ionic" interactions are traditionally used to describe the chemical bonding. For our systems we report the results of calculations where the orbital occupation of the metal atom orbitals is appropriate for the correct spin state. Thus, for example, in the Mn(II) system with its high-spin (hs) d^5 configuration, all of the largely metal-located d orbitals are singly occupied.

The results of the calculations for the (Ca,Mg)O and (M,Mg)O systems where M = Mn, Fe, or Co, are in accord with experiment concerning the positive sign of $\Delta H'_{xs}(y)$.[2-6] Very satisfyingly the computed result for the (Ni,Mg)O solid solution shows a negative $\Delta H'_{xs}(y)$ in accord with the experimental work of Navrotsky and Davies.[7] Experimentally the excess energy curve for (Ni,Mg)O is found to be asymmetric toward the MgO end member, i.e., higher measured excess energy for a Mg-rich (Ni,Mg)O solid

(28) Vaknin, D.; et al. *Phys. Rev. Lett.* **1987**, *58*, 2802.
(29) See, for example: Goodenough, J. B. *Magnetism and The Chemical Bond*; Wiley-Interscience: New York, 1963.

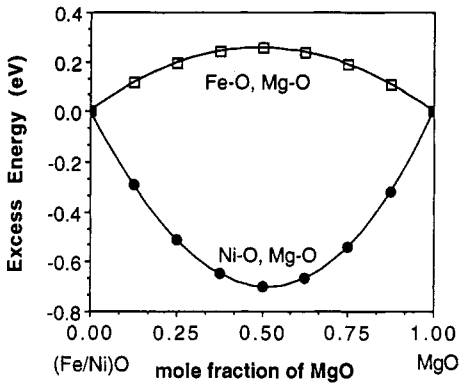

Figure 10. Computed total excess energy curves for (a) (Fe,Mg)O and (b) (Ni,Mg)O generated from the diatomic model.

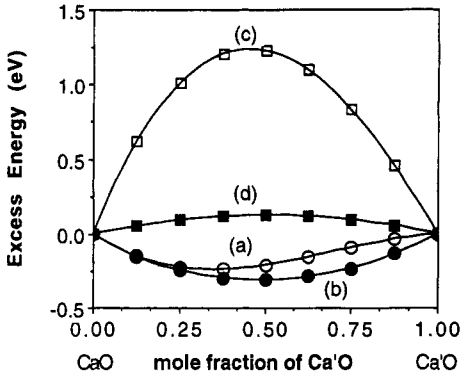

Figure 11. Calculations designed to show the effect of "size". The total excess energy curves for (Ca,Ca')O generated from the solid-state calculation and from the diatomic model. Metal orbitals of Ca' are contracted and used in (a) diatomic model and (b) the solid-state model. Metal orbitals of Ca' are enlarged and used in (c) diatomic model and (d) the solid-state model.

solution than for an equivalent Ni-rich solution. We also find, in Figure 3b, similar asymmetry in our calculated data, though the degree of asymmetry is not as large as that from experiment. This theoretical calculation of a negative $\Delta H'_{xs}(y)$ is a very important result. No other model has had any success in this area. Such negative deviations from Raoultian behavior are not accounted for in the Navrotsky and Davies' correlation with ΔV noted above. Most isostructural binary solid solutions of metal oxides[2-6,11] and metal sulfides[30] exhibit positive excess enthalpies of mixing. Negative deviations, however, are also found for the (Co,Mg)TiO_3 solution, and this observation along with that for (Ni,Mg)O has been suggested to be a result of electron configuration effects alone,[7,11] a conclusion we find support for below. The negative deviations found in the spinel solutions $(Co,Mg)_2TiO_4$ and $(Ni,Mn)_2SiO_4$ though may be a result of a cation redistribution and the analogous deviations in the olivine solution $(Ni,Mg)_2SiO_4$ may be a consequence of an ordering of cations on the octahedral M1 and M2 sites.[11,20] Newton and Wood[20] have described the cation ordering in $(Ni,Mg)_2SiO_4$ in terms of crystal-field stabilization energy.

Listed in Table I are the metal oxides, their lattice parameters, the metal–oxygen distances, and experimental values of W or A and B collected by Davies and Navrotsky.[11] For comparison, we have also listed our calculated values for the corresponding solid solutions, fitting the weighted excess energies determined from our

(30) Skinner, B. J.; Luce, F. D. *Am. Miner.* 1971, *56*, 1269.

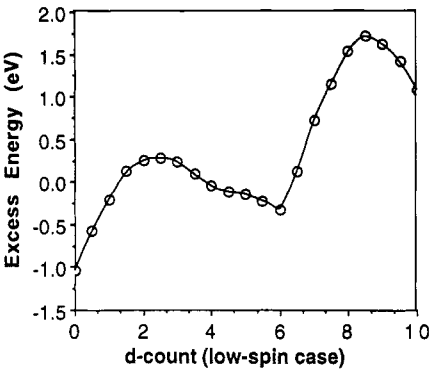

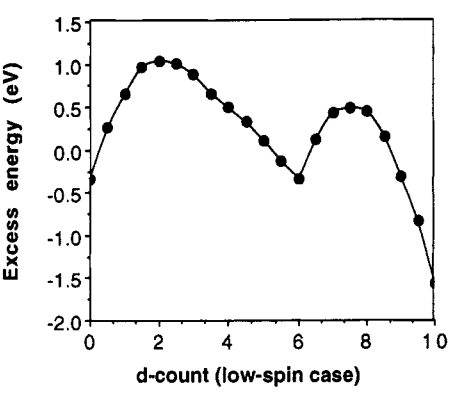

Figure 12. Total excess energy versus low-spin d count of a 50/50 (M,Mg)O solid solutions where M = Fe (a) and Ni (b).

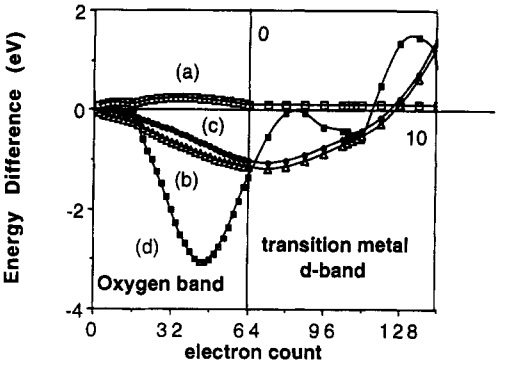

Figure 13. Volume-change processes: stretching Mg_8O_8 and compressing Fe_8O_8. Shown are energy difference or excess energy curves derived from (a) VC2 process, (b) VC1 process, (c) total volume-change process, and (d) actual total excess energetic process of the (Fe,Mg)O solution 4c. The vertical lines adjacent to the labels 0 and 10 mark the electron counts appropriate for d^0 and d^{10} configurations.

extended Hückel treatment to the regular and/or subregular model wherever appropriate. Notice that, for most cases, our calculated values are about twice as large as the experimental ones. For (Ni,Mg)O, we can fit our data to a subregular model, though our excess energy curve is only slightly asymmetric toward MgO, unlike the actual experimental finding which has indicated a more prominent asymmetry toward the MgO end member.[7] Fitting both the calculated and experimental values for the (Ni,Mg)O system to a regular model, leads to a calculated W about 3 times as large as that derived from experiment. For the highly ionic metal oxide solutions the calculated value of W is only about one-fourth of that generated from experiment. Such poor quantitative agreement is hardly unexpected from a one-electron model where bond lengths change.

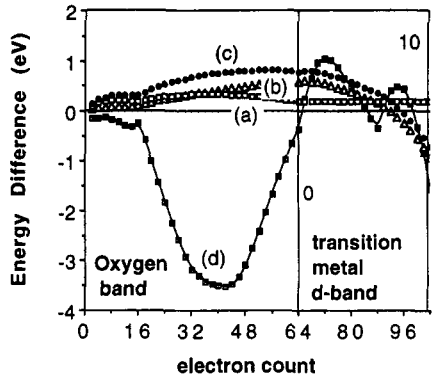

Figure 14. Volume-change processes: stretching Ni_8O_8 and compressing Mg_8O_8. Displayed herein are energy difference or excess energy curves derived from (a) VC2 process, (b) VC1 process, (c) total volume-change process, and (d) sum total excess energy for the (Ni,Mg)O solution 4c. The vertical lines adjacent to the labels 0 and 10 mark the electron counts appropriate for d^0 and d^{10} configurations.

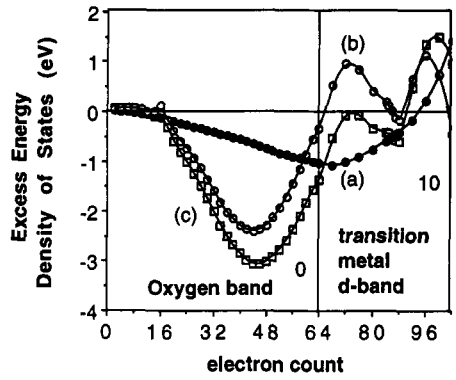

Figure 15. Decomposition of the total excess energy of solution $Fe_4Mg_4O_8$-type 4c. (a) total volume-change process, (b) total metallic substitution process, and (c) sum total excess energy for the (Fe,Mg)O solution 4c. The vertical lines adjacent to the labels 0 and 10 mark the electron counts appropriate for d^0 and d^{10} configurations.

The calculated results of Figures 3 and 4 show some interesting trends. In the series M = Mn, Fe, Co, the amplitude of the $\Delta H'_{xs}(y)$ curve for (M,Mg)O solid solutions decreases and the curves become more asymmetric or subregular toward the MgO end member. Notice also that for the series there is a concomitant decrease in M–O distances as shown in Table I.

It is interesting to contrast these results with the predictions of the simplest ionic model. Inclusion of a Végard law-like change in lattice constant into a Madelung calculation of the electrostatic energy leads to the calculated $\Delta H'_{xs}(x)$ plot of Figure 5. The energy scale is arbitrary and depends upon the difference in internuclear separation (Δr) of the end-members. Notice the (small) asymmetry toward the system with the *shorter* internuclear distance. This is reflected in the higher excess lattice energy required to put the larger guest ion into the lattice of smaller host ions, noted by Fancher and Barsch.[13] Such asymmetry is in contrast to the results of Figures 3 and 4. The dependence of the maximum in this plot, $\Delta H'_{xs}(0.5)$, on Δr on this simple ionic model is shown in Figure 6. Importantly it does not allow ΔH_{xs} ever to be negative. Figure 7 shows a plot of the experimentally determined values of W versus Δr. There is a rough correlation between the two, increasingly larger values of W being found for the increasingly larger Co, Fe, and Mn. On mixing the oxides of these three transition metals (Mn, Fe, and Co)

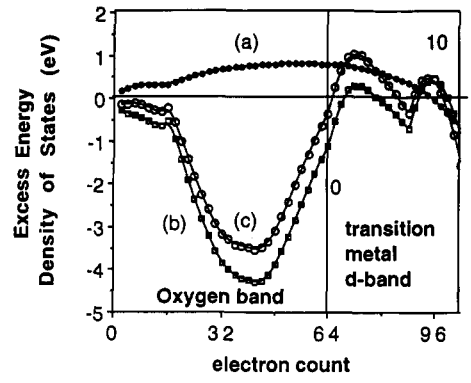

Figure 16. Decomposition of the total excess energy of solution $Ni_4Mg_4O_8$-type 4c: (a) total volume-change process, (b) total metallic-substitution process, and (c) sum total excess energy for the (Ni,Mg)O solution 4c. The vertical lines adjacent to the labels 0 and 10 mark the electron counts appropriate for d^0 and d^{10} configurations.

with MgO, whose M–O distance is 2.1060 Å, these three transition-metal ions find themselves in a smaller environment. We would expect that on almost any "size" model, as the difference in the metal–oxygen distance of the end members becomes larger, the strain becomes greater and the excess energy curve more asymmetric. The calculated asymmetry however, becomes more pronounced as the size difference of the two end members decreases. Along with the result of a negative value of $\Delta H'_{xs}(0.5)$ for (Ni,Mg)O shown in Figure 7, it is clear that size cannot be the whole story here.

An improved classical model comes from molecular mechanics by including a short-range repulsion and van der Waals attractive force in addition to the electrostatic forces,[31,32] as in eq 10. The potential parameters used in

$$\mathrm{LE} = \sum_{i<j}[(q_i q_j/r_{ij}) + A\exp(-r_{ij}/\rho_{ij}) - (C_{ij}/r_{ij}^6)] \quad (10)$$

our lattice energy calculation are taken from refs 33 and 34 and are listed in Table VI. These calculations of course do not contain any dependence on d orbital occupancy *per se*. Some of the results are illustrated in Figures 8 and 9. Since the charges on all of these ions is 2+, it is the differences in the nonelectrostatic part of the interaction potential which leads to the splitting apart in energy of the points associated with the different solid solutions of the same stoichiometry. Notice that when M = Ca (or Mn, but this case is not shown), a well-defined asymmetry is seen toward the MgO end-member (the species with the smaller lattice constant), a consequence of the ionic model. But importantly notice the failure of the more sophisticated calculation to give a negative $\Delta H'_{xs}(y)$ for the (Ni, Mg)O solid solution. Here the calculated curve is small but positive, not an unexpected result since the potential parameters of Ni^{2+} and Mg^{2+} are quite similar.

A Diatomic Model

We may regard the generation of $\Delta H'_{xs}(y)$ as originating from the sum of two processes, the energetics associated with the volume change of the two components plus the

(31) Driessens, F. C. M. *Ber. Bunsen-Ges. Phys. Chem.* **1968**, *72*, 764.
(32) (a) Dunitz, J. D.; Orgel, L. G. *Phys. Chem. Solids* **1957**, *3*, 311. (b) Burnham, C. W. In ref 1b.
(33) Lewis, G. V.; Catlow, C. R. A. *J. Phys. C: Solid State Phys.* **1985**, *18*, 1149.
(34) Catlow, C. R. A. *Proc. R. Soc. London A* **1977**, *353*, 533.

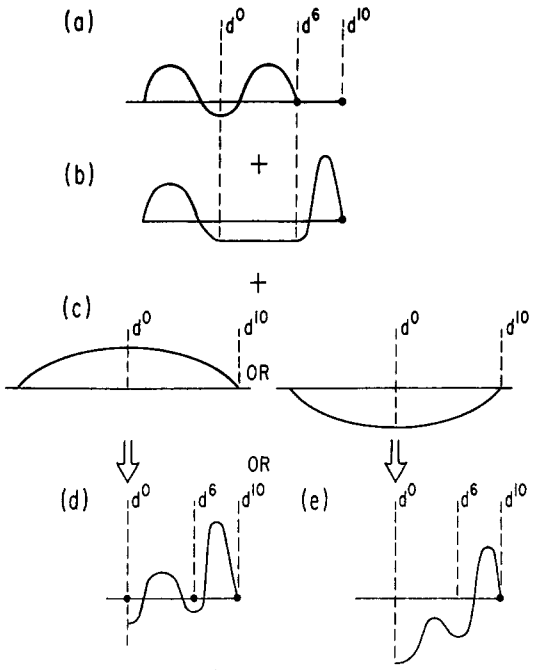

Figure 17. Interpretation of the excess energy plots in terms of moments. (a, b). Expected shape from consideration of the fourth moment effects in σ and π manifolds. The flat portions represent the σ or π nonbonding regions of the density of states. (c) The two possible contributions from the second moment effect. (d, e) How addition of (a), (b), and (c) leads to energy difference curves similar to those found by calculation in Figures 15 and 16.

metallic substitution process at the new distance appropriate for the composition under consideration. We will investigate both in detail in the next section, but here we will ignore the second term and ask about the electronic ingredients which go into the volume change on our one-electron orbital model. It will be useful to consider the energetics accompanying changes in the AO and BO distances using the simplest possible pairwise (two-atom) interaction model. In terms of the number of nearest neighbors, N, the energies at $x = 0, 1$ are $E(x=0) = NP[\mathrm{AO}]$ and $E(x=1) = NQ[\mathrm{BO}]$, where $P[\mathrm{AO}]$ and $Q[\mathrm{BO}]$ are respectively the pairwise energy of the diatomic A–O at the AO distance, and the pairwise energy of the diatomic B–O at the BO distance. With Raoultian ideality, although

$$E_{\mathrm{ideal}}(x) = (1-x)NP[\mathrm{AO}] + xNQ[\mathrm{BO}] \quad (11)$$

the actual energies of specific compositions are of the form

$$E_{\mathrm{actual}}(x) = (1-x)NP[\mathrm{A}_x\mathrm{B}_{1-x}\mathrm{O}] + xNQ[\mathrm{A}_x\mathrm{B}_{1-x}\mathrm{O}] \quad (12)$$

where $P[\mathrm{A}_x\mathrm{B}_{1-x}\mathrm{O}]$ and $Q[\mathrm{A}_x\mathrm{B}_{1-x}\mathrm{O}]$ are respectively the A–O and B–O pairwise energies at the distance appropriate for a given $\mathrm{A}_x\mathrm{B}_{1-x}\mathrm{O}$ composition. Writing a quadratic dependence for the interaction potential

$$P[\mathrm{A}_x\mathrm{B}_{1-x}\mathrm{O}] = (A + xa + x^2\alpha) \quad (13)$$

$$Q[\mathrm{A}_x\mathrm{B}_{1-x}\mathrm{O}] = (B + (1-x)b + (1-x)^2\beta) \quad (14)$$

leads to the excess energy of mixing

$$\Delta E'_{\mathrm{xs}}(X) = x(1-x)N[(a+b) + x\alpha + (1-x)\beta] \quad (15)$$

We can use perturbation theory within the molecular orbital framework to identify a, b, α, and β with relevant orbital parameters. From second-order perturbation theory, the pairwise interaction energy between two orbitals i and j located on the atoms A and O is given by

$$P_{ij} = (H_{ij})^2/(H_{ii} - H_{jj}) \quad (16)$$

Using the Wolfsberg–Helmholtz approximation $H_{ij} = k(S_{ij})(H_{ii} + H_{jj})/2$

$$P_{ij} = k^2(S_{ij})^2(H_{ii} + H_{jj})^2/4(H_{ii} - H_{jj}) = \mathbf{H}(S_{ij})^2 \quad (17)$$

Expansion of S_{ij} as a function of the change in A–O distance as the metal composition x varies between 0 and 1 leads to

$$P_{ij} = \mathbf{H}[(S_{ij}(x=0))^2 + 2(S_{ij}(x=0))(\mathrm{d}S_{ij}/\mathrm{d}x)x + x^2\{(\mathrm{d}^2S_{ij}/\mathrm{d}x^2)(S_{ij}(x=0)) + (\mathrm{d}S_{ij}/\mathrm{d}x)^2\}] \quad (18)$$

Analogously for the orbitals j,k centered on O and B:

$$Q_{jk} = \mathbf{H}[(S_{jk}(x=1))^2 + 2(S_{jk}(x=1))(\mathrm{d}S_{jk}/\mathrm{d}(1-x))(1-x) + (1-x)^2\{(\mathrm{d}^2S_{jk}/\mathrm{d}(1-x)^2)(S_{jk}(x=1)) + (\mathrm{d}S_{jk}/\mathrm{d}(1-x))^2\}] \quad (19)$$

$P[\mathrm{A}_x\mathrm{B}_{1-x}\mathrm{O}]$ and $Q[\mathrm{A}_x\mathrm{B}_{1-x}\mathrm{O}]$ are then simply the weighted (by the electron occupancy) sums of the orbital interactions of 5 taking into account the orbital occupancy. Using

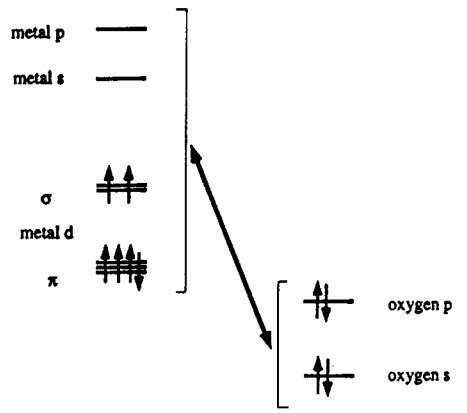

5

this model it is easy to see from eq 15 that if there is no change in volume (a, b, α, and $\beta = 0$) then $\Delta E'_{\mathrm{xs}}(x)$ (defined in the same way as $\Delta H'_{\mathrm{xs}}(x)$) = 0.

For the process where the terminal solutions have different unit cell volumes, using eqs 37–40, we can now define the following parameters:

$$a = \sum \mathbf{H}[2(S_{ij}(x=0))(\mathrm{d}S_{ij}(A-O)/\mathrm{d}x))] \quad (20)$$

$$\alpha = \sum \mathbf{H}[(\mathrm{d}^2S_{ij}(A-O)/\mathrm{d}x^2)(S_{ij}(x=0)) + (\mathrm{d}S_{ij}(A-O)/\mathrm{d}x)^2] \quad (21)$$

$$b = \sum \mathbf{H}[2(S_{ij}(x=1))(\mathrm{d}S_{ij}(B-O)/\mathrm{d}(1-x))] \quad (22)$$

$$\beta = \sum \mathbf{H}[(\mathrm{d}^2S_{ij}(B-O)/\mathrm{d}(1-x)^2)(S_{ij}(x=1)) + (\mathrm{d}S_{ij}(B-O)/\mathrm{d}(1-x))^2] \quad (23)$$

where the summation represents the electron occupancy weighted sums taking into account the occupancy of 5. All four parameters may be readily evaluated numerically for each case. Calculated $\Delta E'_{\mathrm{xs}}(x)$ curves are shown in Figure 10.

Such a model clearly reproduces the signs of ΔH_{xs} for the (M,Mg)O systems. As seen in Figure 10, the different behavior of the (Fe,Mg)O and (Ni,Mg)O systems can be mimicked by the diatomic model, which shows that the nature of the transition metal and its d-orbital occupancy

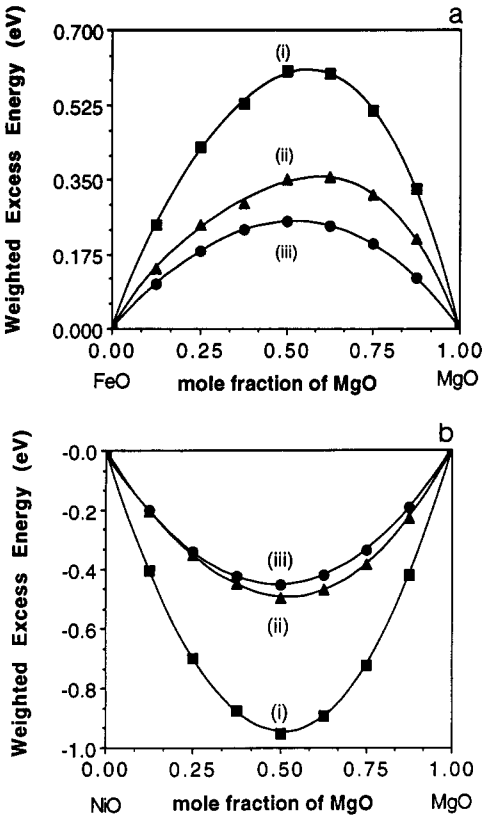

Figure 18. Decomposition of the weighted total excess energy curve of (M,Mg)O solid solution, where M = Fe (a) or Ni (b). (i) Total excess energy curve; (ii) metallic–substitution excess energy curve; (iii) volume-change excess energy curve.

control the sign of $\Delta E'_{xs}(x)$. Not shown are similar plots for (Ca,Mg)O and (Ca,Sr)O. Positive values of $\Delta E'_{xs}(x)$ are calculated for both.

Insight into how atomic "size" appears in the calculation comes from the influence of variation of the orbital parameters of A and B on the sign and shape of the $\Delta E'_{xs}(x)$ curves. We chose the (Ca,Sr)O solid solution for this purpose. Figure 11 shows the results of calculations on a set of (Ca,Ca′)O solid solutions where the hypothetical Ca′O system has the lattice parameter of SrO. The valence s and p orbitals of Ca′ are either contracted or expanded by about 10–20% with respect to the values for Ca. Interestingly they show how a negative ΔH_{xs} curve may be generated. The excess energy for the "orbitally contracted" (Ca,Ca′)O solid solution is negative but that for the case where the metal orbitals of Ca′ are expanded is positive (curve d). Qualitatively similar results are found using the diatomic model but with somewhat different amplitudes. Here is the orbital analog of the "size" effect. Contraction of an orbital by increasing its Slater exponent leads to a smaller atom while the converse leads to a larger one. Negative ΔH_{xs} values will not be seen for systems of this type in practice since Ca′O has a longer Ca′–O distance than CaO and this automatically corresponds to the case with the smaller exponent and thus expanded wave function.

Importance of d Count

The results described in Figures 3 and 4 lead to the obvious question as to whether they are specifically associated with Fe or with Ni for example or whether there is a simple dependence on d-count in a rigid band sense. Figure 12a shows the calculated $\Delta H'_{xs}\{M_4Mg_4O_8\}_{4c}$ plot for a specific $Fe_4Mg_4O_8$ solid solution (the arrangement 4c in Figure 2) as a function of low-spin d count. Figure 12b shows the analogous plot calculated for the corresponding $Ni_4Mg_4O_8$ solid solution. The general behavior is independent of the choice of solid solution. Both plots show an oscillating function superimposed on an increasing or decreasing background. Notice that the oscillations appear to take place around the points d^0, d^6, and d^{10}, three interesting d counts from the point of view of the orbital structure of the octahedron. But while the general behavior of both systems is similar, there are important quantitative differences between the two which are important in controlling the $\Delta H'_{xs}(y)$ values for the real high-spin systems. For example, $\Delta H'_{xs}\{M_4Mg_4O_8\}_{4c}$ for the hsd^6 (Fe,Mg)O system, type 4c, is positive (Figure 3), a value equal to one-half of the sum of the excess energies at lsd^2 and d^{10} using the approach described earlier. As one can see in Figure 12a, the d^{10} excess energy value is positive whereas the lsd^2 excess energy is negative but smaller in magnitude. Therefore, the value of $\Delta H'_{xs}(y)$ for hsd^6 is small and positive. The excess energy of the (Ni,Mg)O system (hsd^8) was found to be negative (Figure 3), a result predictable from the sign and magnitude of the excess energies at hsd^6 and d^{10} from Figure 12b, both of which are indeed in the negative range.

Oscillating behavior with electron count of this type may be understood in a very general way using the method of moments as we will seen in the next section. However, the fact that $\Delta H'_{xs}\{M_4Mg_4O_8\}_{4c}$ increases as a function of d count in Figure 12a but descends in Figure 12b is clearly important in controlling the magnitude of the energy changes and is easy to understand. The metal d orbitals which are being filled at this point are metal–oxygen antibonding. Thus a contraction of the MO distance on forming the solid solution will lead to an increasingly antibonding (destabilizing) contribution with d count, and an expansion of this distance the converse. Thus the observed slopes of the background in Figure 12 are commensurate with the decrease in unit cell volume on going from FeO to MgO (a = 4.3057–4.2121 Å) but an increase on going from NiO to MgO (a = 4.1684–4.2121 Å).

Volume Change and Metallic Substitution

In this section we will quantify the ideas described above by evaluation of the energy changes associated with the two processes shown in 6,namely the volume change (VC1,

6

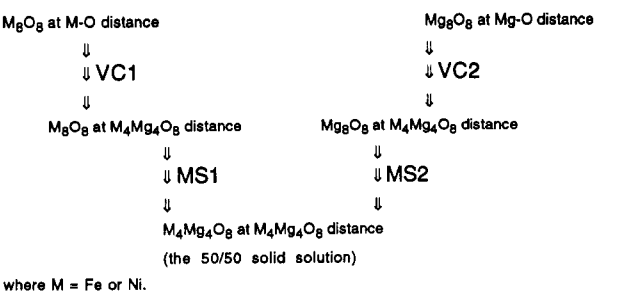

VC2) and metallic substitution (MS1, MS2) reactions. For a specific permutation (we chose the 50/50 permutation

Table II. Actual and Excess Cis- and Trans-Three-Atom Contributions in $A_{8-y}B_yO_8$

solution	type[a]	cAOA and (xscAOA)	cAOB and (xscAOB)	cBOB and (xscBOB)	tAOA and (xstAOA)	tAOB and (xstAOB)	tBOB and (xstBOB)
A_8O_8	0	96 (0)	0 (0)	0 (0)	24 (0)	0 (0)	0 (0)
A_7BO_8	1	72 (−12)	24 (24)	0 (−12)	20 (−1)	2 (2)	2 (−1)
$A_6B_2O_8$	2a	48 (−24)	48 (48)	0 (−24)	18 (0)	0 (0)	6 (0)
	2b	48 (−24)	48 (48)	0 (−24)	16 (−2)	4 (4)	4 (−2)
	2c	56 (−16)	32 (32)	8 (−16)	16 (−2)	4 (4)	4 (−2)
	2d	52 (−20)	40 (40)	4 (−20)	16 (−2)	4 (4)	4 (−2)
$A_5B_3O_8$	3a	32 (−28)	56 (56)	8 (−28)	14 (−1)	2 (2)	8 (−1)
	3b	32 (−28)	56 (56)	8 (−28)	14 (−1)	2 (2)	8 (−1)
	3c	40 (−20)	40 (40)	16 (−20)	12 (−3)	6 (6)	6 (−3)
	3d	32 (−28)	56 (56)	8 (−28)	12 (−3)	6 (6)	6 (−3)
$A_4B_4O_8$	4a	16 (−32)	64 (64)	16 (−32)	12 (0)	0 (0)	12 (0)
	4b	32 (−16)	32 (32)	32 (−16)	8 (−4)	8 (8)	8 (−4)
	4c	20 (−28)	56 (56)	20 (−28)	10 (−2)	4 (4)	10 (−2)
	4d	24 (−24)	48 (48)	24 (−24)	10 (−2)	4 (4)	10 (−2)
	4e	24 (−24)	48 (48)	24 (−24)	8 (−4)	8 (8)	8 (−4)
	4f	16 (−32)	64 (64)	16 (−32)	10 (−2)	4 (4)	10 (−2)
	4g	16 (−32)	64 (64)	16 (−32)	8 (−4)	8 (8)	8 (−4)
$A_3B_5O_8$	5a	8 (−28)	56 (56)	32 (−28)	8 (−1)	2 (2)	14 (−1)
	5b	8 (−28)	56 (56)	32 (−28)	8 (−1)	2 (2)	14 (−1)
	5c	16 (−20)	40 (40)	40 (−20)	6 (−3)	6 (6)	12 (−3)
	5d	8 (−28)	56 (56)	32 (−28)	6 (−3)	6 (6)	12 (−3)
A_2B36O_8	6a	0 (−24)	48 (48)	48 (−24)	6 (0)	0 (0)	18 (0)
	6b	0 (−24)	48 (48)	48 (−24)	4 (−2)	4 (4)	16 (−2)
	6c	8 (−16)	32 (32)	56 (−16)	4 (−2)	4 (4)	16 (−2)
	6d	4 (−20)	40 (40)	52 (−20)	4 (−2)	4 (4)	16 (−2)
AB_7O_8	7	0 (−12)	24 (24)	72 (−12)	2 (−1)	2 (2)	20 (−1)
B_8O_8	8	0 (0)	0 (0)	96 (0)	0 (0)	0 (0)	24 (0)

[a] For any $A_{8-y}B_yO_8$ solid solution, A = M and B = Mg. Each solid solution is labeled with a type (0, 1, 2a, ..., 6d, 7, or 8) to indicate its unique arrangement as described in Figure 1.

Table III. Numbers and Weights of Three Atom Terms, *P* and *Q*, in $A_{8-y}B_yO_8$ Solid Solutions

solution	type	P^a	Q^b	$wt-P$	$wt-Q$	$(wt-P+wt-Q)$
A_7BO_8	1	12	1	12.000	1.000	13.000
$A_6B_2O_8$	2a	24	0	20.571	1.714	22.285
	2b	24	2			
	2c	16	2			
	2d	20	2			
$A_5B_3O_8$	3a	28	1	25.714	2.143	27.857
	3b	28	1			
	3c	20	3			
	3d	28	3			
$A_4B_4O_8$	4a	32	0	27.429	2.286	29.714
	4b	16	4			
	4c	28	2			
	4d	24	2			
	4e	24	4			
	4f	32	2			
	4g	32	4			
$A_3B_5O_8$	5a	28	1	25.714	2.143	27.857
	5b	28	1			
	5c	20	3			
	5d	28	3			
$A_2B_6O_8$	6a	24	0	20.571	1.714	22.286
	6b	24	2			
	6c	16	2			
	6d	20	2			
AB_7O_8	7	12	1	12.000	1.000	13.000

[a] P = number of $\{2\cdot xscis_{AOB} - xscis_{AOA} - xscis_{BOB}\}$, the subset of excess cis-three-atom terms. [b] Q = number of $\{2\cdot xstrans_{AOB} - xstrans_{AOA} - xstrans_{BOB}\}$, the subset of excess trans-three-atom terms.

4c again) we can write

$$\Delta H'_{xs}\{M_4Mg_4O_8\}_{4c} = 0.5(VC1 + VC2) + 0.5(MS1 + MS2)$$

$$= \Delta H_{VC} + \Delta H_{MS} \quad (24)$$

where VCi is the energy change associated with contracting or expanding the structure as appropriate from the end-member geometry (M–O or Mg–O) using Végard's rule, and MCi is the energy change engendered by the replacement of half of the metal atoms by atoms of the other type.

Table IV. Calculated Energies Φ_P and Φ_Q Associated with Subsets of Cis- and Trans-Three-Atom Terms in (M,Mg)O Solid Solutions

			$W_{(M,Mg)O}$	
solution	$\Phi_P{}^a$ (eV)	$\Phi_Q{}^b$ (eV)	eV/mol	kJ/mol
(Ca,Mg)O	−0.001 57	−0.007 26	0.174	16.8
(Mn,Mg)O	−0.006 52	−0.029 04	0.412	39.7
(Fe,Mg)O	+0.017 87	−0.055 08	0.307	29.6
(Co,Mg)O	−0.005 80	−0.034 78	0.084	8.1
(Ni,Mg)O	−0.016 89	−0.014 62	−0.473	−45.6

[a] Energy associated with P, the number of $\{2\cdot xscis_{AOB} - xscis_{AOA} - xscis_{BOB}\}$, the subset of excess cis-three-atom terms. [b] Energy associated with Q, the number of $\{2\text{-}xstrans_{AOB} - xstrans_{AOA} - xstrans_{BOB}\}$, the subset of excess trans-three-atom terms.

The results are shown in Figure 13 and show that the sloping background is associated with the change in volume and the oscillations with the metallic substitution process. Such results are readily understood from the method of moments.[35,36] The number of nodes expected in the range encompassing orbital filling from the deepest-lying bonding orbital to the highest-lying antibonding orbital is equal to the order of the first disparate moment in the electronic density of states. The moments of the energy density of states may be expressed in terms of the sums of weighted walks around the lattice, and so the number of nodes found in some ΔE plot between two structures as a function of electron count tells us about the topological features underlying the difference in energy. Using these ideas the form of the plot expected from the volume change alone is a second moment one since the energetics associated with the change in distance are just two-atom ones. In the moments language this arises since it is a

(35) Burdett, J. K.; Lee, S. *J. Am. Chem. Soc.* **1985**, *107*, 3050, 3063.
(36) Burdett, J. K. *Struct. Bonding* **1987**, *65*, 30.

Table V. Orbital Parameters Used in Band Structure Calculations[a]

atom	orbital	H_{ii} (eV)	ζ_{i1}	(c_1)	ζ_{i2}	(c_2)
Mg	3s	−8.00	1.04			
	3p	−5.00	1.04			
Ca	4s	−7.00	1.10			
	4p	−4.00	1.10			
Mn	4s	−9.75	0.97			
	4p	−5.89	0.97			
	3d	−11.67	5.15	(0.5139)	1.70	(0.6929)
Fe	4s	−9.10	1.9			
	4p	−5.32	1.9			
	3d	−12.6	5.35	(0.5505)	2.00	(0.6260)
Co	4s	−9.21	2.0			
	4p	−5.29	2.0			
	3d	−13.18	5.55	(0.5680)	2.10	(0.6060)
Ni	4s	−9.17	1.825			
	4p	−5.15	1.125			
	3d	−13.49	5.75	(0.5683)	2.00	(0.6292)
O	2s	−32.3	2.275			
	2p	−14.8	2.275			

[a] From *Table of Parameters for Extended Hückel Calculations*; collected by Santiago Alvarez, Barcelona, 1985.

walk of length 2 which links an atom with its neighbors (7)and thus a ΔE plot with two nodes. Expansion of the

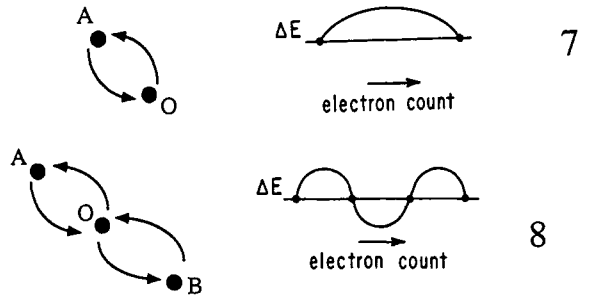

MgO lattice from the end-member distance of 2.1060 Å to the 50/50 (Fe/Mg)O distance of 2.1294 Å costs energy. However, compressing FeO from the end-member distance of 2.1528 Å to the 50/50 (Fe/Mg)O distance of 2.1294 Å is an energetically favorable process. Their sum is a second moment curve (Figure 13, curve c) with a negative amplitude over most of its range. Such a plot is easily understood in another way from the general bonding characteristics of these oxides. The largely oxide bands are bonding between metal and oxygen, but the largely metal d levels are antibonding. Filling the orbitals up to d^0 fills all the bonding orbitals and leads to maximum bonding. Past d^0, antibonding orbitals are filled and the bond order drops. Compressing the energetically dominant Fe–O linkages increases metal–oxygen interactions, increases the bonding character of the bonding orbitals and increases the antibonding character of the metal d orbitals. This leads to a maximum in the amplitude of this plot at around d^0. Comparable results for the (Ni,Mg)O system are illustrated in Figure 14. Compressing MgO from the end-member value of 2.1060 Å to the Végard 50/50 (Ni,Mg)O value of 2.0901 Å gives a weak second-moment curve (Figure 14, curve a), similar, but opposite in sign, to that found above for stretching MgO to the Végard 50/50 (Fe,Mg)O distance. Stretching NiO from the end-member value of 2.0842 Å to the Végard 50/50 (Ni,Mg)O distance of 2.0951 Å leads to a stronger second-moment curve (Figure 14, curve b) which is largely positive over its range, for reasons exactly analogous to those described above. The overall curve (Figure 14, curve c) is a second-moment curve, with the opposite phase to that for (Fe,Mg)O.

Table VI. Potential Parameters Used in Lattice Energy Calculations[a]

cation	charge	A (eV)	ρ (Å)
Mg	2	1428.5	0.2945
Ca	2	1090.4	0.3437
Mn	2	1007.4	0.3262
Fe	2	1207.6	0.3084
Co	2	1491.7	0.2951
Ni	2	1582.5	0.2882

anion	charge	A (eV)	ρ (Å)	C (eV Å)
O	2	22764.3	0.1490	112.2

[a] From refs 33 and 34. For the metal ions these parameters refer to metal–oxygen interactions. For oxygen they refer to oxygen–oxygen interactions.

Figures 15 and 16 show the effect of metallic substitution for (Ni,Mg)O and (Fe,Mg)O, respectively, and show the origin of the oscillating behavior of $\Delta H'_{xs}\{M_4Mg_4O_8\}_{4c}$ with d count. We can view these curves using the moments ansatz in a way similar to studies[37] of the ordering patterns of the defects in perovskites. For A to "see" B in an AOB solid a walk of length four is needed (8) with four nodes in the plot. Since there are two separate bonding networks (σ and π) in this system we can draw the expected form of the plots as in Figure 17. To the left of d^0 there is no energetic separation of σ, π, and nonbonding orbital manifolds and such details of the oscillations are washed out. They are not shown in the composite plots. The MO π^*-manifold (filling the t_{2g} block from d^0 to lsd^6) and the MO σ^*-manifold (filling the e_g block from lsd^6 to d^{10}) are regarded as half of a fourth moment plot. In the defect perovskite case of ref 37, with an eighth moment problem overall, these two manifolds contain half of an eighth moment curve. These curves are what would be expected on a Hückel model without overlap. The reader can clearly see the effect of overlap in Figures 15 and 16, which change the details of this electronic decomposition but not the general form. There are some general rules from the moments method which often allow us to predict the sign of the fourth moment plot.[35,36] When the energies of two systems are being compared, it is the one with the larger fourth moment which is more stable for the earliest electron counts. In our case here we cannot make analogous predictions, since there are three separate (AO, BO, and $A_xB_{1-x}O$) densities of states to be considered. This is a problem we have discussed elsewhere.[38,39]

An interesting result is shown in Figure 18. It shows for the two systems (Fe,Mg)O and (Ni,Mg)O, the breakdown of $\Delta H'_{xs}(y)$ into the energy change associated with the volume change and that associated with the metallic substitution. Notice that they are of approximately equal magnitude from the calculation and that the asymmetry only appears in the metallic substitution contribution.

Potential Parameters

It is now clear that ΔH_{xs} may profitably be written as a sum of the energetics associated with a change in volume and those associated with the metallic substitution process as in eq 24. The first term only involves changes in the two-atom interactions M–O or Mg–O, whereas the second

(37) Burdett, J. K.; Kulkarni, G. V. *J. Am. Chem. Soc.* **1988**, *110*, 5361.
(38) Burdett, J. K.; Fässler, T. F. *Inorg. Chem.* **1991**, *30*, 2859.
(39) Heine, V.; Robertson, I. J.; Payne, M. C. *Bonding and Structure of Solids*; Haydock, R., Inglesfield, J. E., Pendry, J. B., Eds.; The Royal Society: London, 1991.

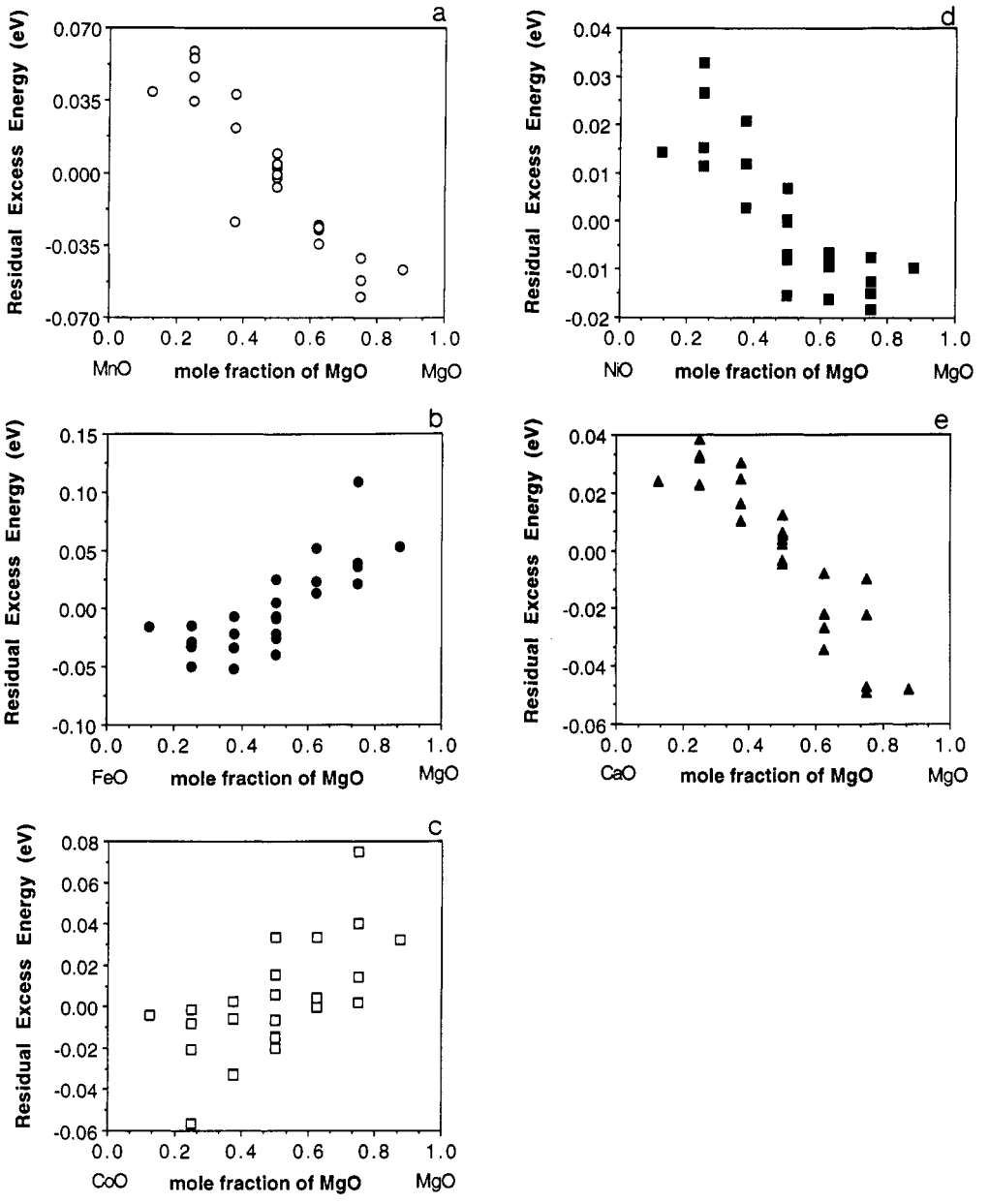

Figure 19. Residual excess energies of (M,Mg)O solid solutions after fitting to subsets P and Q, where M = Mn, Fe, Co, Ni, and Ca and P and Q are the respective number of excess cis- and trans-three-body walks. M = (a) Mn; (b) Fe; (c) Co, (d) Ni, and (e) Ca.

term involves or three-atom and higher interactions, M–O–Mg, M–O–Mg–O–M, etc., interactions. The form of the regular solution eq 1 suggests that ΔH_{MS} (or the three-atom terms which contribute to it) should be accessible by an expression of this sort. Equation 1 in fact needs to be expanded to include the potential parameters of both *cis* and *trans* types. The actual number of three-atom potential parameters, of both *cis*- and *trans* types, for all 25 $A_{8-y}B_yO_8$ solid solutions (A = M and B = Mg) and the two end-members (A_8O_8 and B_8O_8) are listed in Table II. Also shown are the excess values or the deviations from ideal behavior. Just as the combination $\phi_{AA} + \phi_{BB} - 2\phi_{AB}$ represented a single parameter there, so the analogous parameters, $\Phi_P = \{2\phi\ cis_{AOB} - \phi\ cis_{AOA} - \phi\ cis_{BOB}\}$ and $\Phi_Q = \{2\phi\ trans_{AOB} - \phi\ trans_{AOA} - \phi\ trans_{BOB}\}$ hold here and may be fitted by knowing the energies of the 27 geometric permutations. Just as before they lead to the $(x)(1-x)$ dependence that is the trademark of the regular solution model, as shown by the weights in the last column of Table III. Recognition of such a quadratic function leads to determination of these two sets of potential parameters (Table IV) and to the residual (cubic and higher) contribution to ΔH_{MS} and thus to ΔH_{xs}. There are many more *cis* than *trans* interactions and so the positive ΔH_{MS} of (Fe,Mg)O is set by the positive value of Φ_P, but both Φ_P and Φ_Q contribute to the negative ΔH_{MS} of (Ni,Mg)O.

The residuals which remain after removal of these terms are often energetically important and are shown in Figure 19. Weighted by the frequency of occurrence of the solid solutions they represent, they are shown in Figure 20. Both the amplitude and sign of the residual depend upon the chemical identity of the system. A rigid-band calculation for a (Fe,Mg)O solid solution obeying Végard's law leads to results which are quite similar to those of Figure 20. In fact the d^0 and d^{10} curves are superimposable, so that the hsd^5 curve, an average of d^0 and d^{10}, behaves similarly to both. Qualitatively similar results are found too from a rigid-band calculation on an (Fe,Mg)O solid solution with constant volume, as expected from the result of Figure 18 which showed that the asymmetry is associated with the metallic substitution. The dependence of the calculated residual energy at $x_{MgO} = 0.25$ and $x_{MgO} = 0.75$ on low-spin

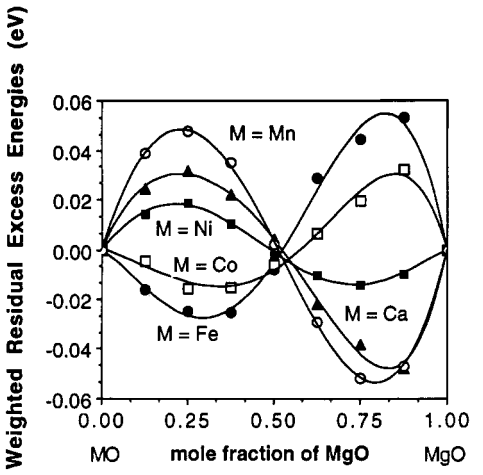

Figure 20. Weighted residual excess energy curves for (M,-Mg)O Solid solutions where M = Ca, Mn, Fe, Co, and Ni.

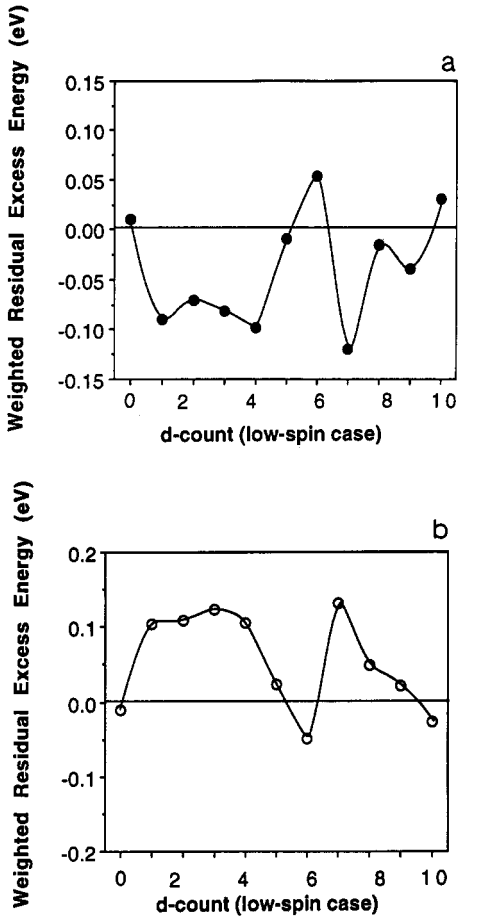

Figure 21. Weighted residual excess energy curves for $Fe_6Mg_2O_8$ and $Fe_2Mg_6O_8$ solid solutions derived from a rigid-band, constant volume calculation: (a) $Fe_6Mg_2O_8$ and (b) $Fe_2Mg_6O_8$.

d count are shown in Figure 21. These two curves, complementary in Fe/Mg composition, fluctuate in an opposing manner along $\Delta E = 0$ as expected from the curves of Figure 20.

Similar behavior is found from calculations on fragments of the rock-salt structure shown in Figure 22. Calculated residual energies for the series of octahedral clusters $Fe_{6-y}Fe'_yO_{19}$ are shown in Figure 23. Fe′ is just an Fe atom in which the d orbitals have been removed so that it only possesses s and p orbitals. The octahedral clusters are the largest of the set and contain one or more combinations of the smaller clusters. The asymmetry in the calculated $\Delta H'_{xs}(y)$ is clearly shown in the weighted residual energy of Figure 23, curves which have been generated in an identical way to those of the solid solutions of the extended array. Clearly the origin of the asymmetry lies at longer range than just A–O–B but is contained in a cluster of this size.

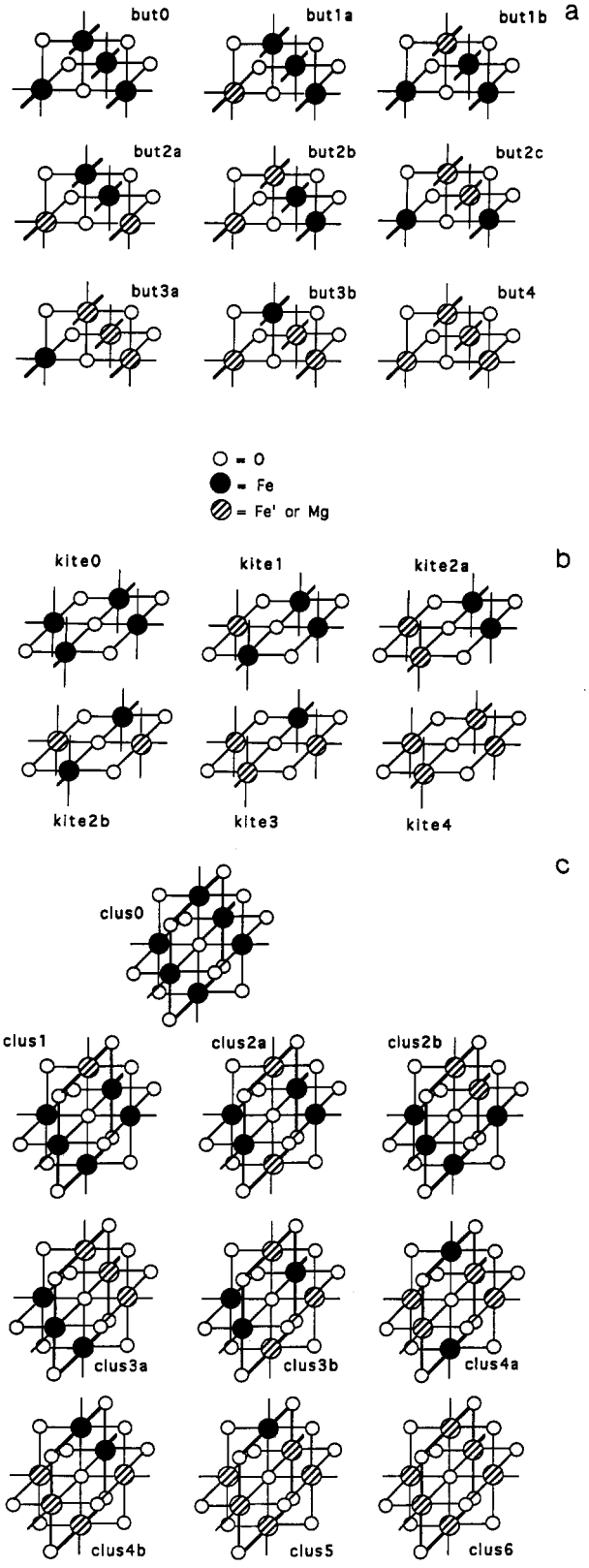

Figure 22. Fragments of the rocksalt-structure as solutions of (a) butterfly, (b) kite, and (c) octahedral clusters. The lines or sticks represent a metal–oxygen bonds as all the metals are octahedrally surrounded by oxygens. The square cluster solutions will be separately illustrated at a later point in this paper.

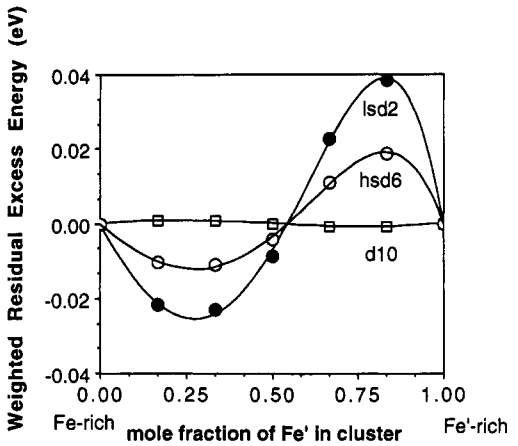

Figure 23. Weighted excess energy curves for $Fe_{6-y}Fe'_yO_{19}$ octahedral cluster solutions at lsd^2, hsd^6, and d^{10}.

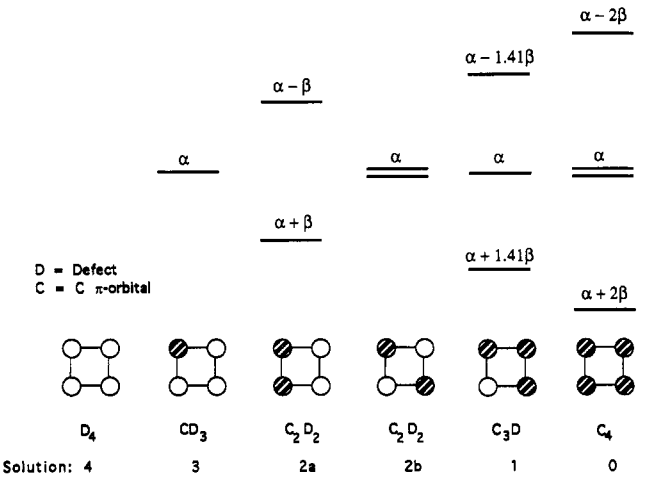

Figure 24. Energy scheme of $C_{4-y}D_y$ π-cluster solutions. From left to right are the cluster solutions D_4 to C_4, with their respective molecular orbital diagram, structure, formula, and solution type.

A model which reveals the origin of these asymmetric features comes from a series of Hückel calculations. We examine a purely hypothetical series of π-clusters $C_{4-y}D_y$, based on a square, where C is a site containing a π-atomic orbital and D is a defect or vacant site with no orbital. This is an attempt to model the effect of replacing a transition metal atom, which carries d orbitals, with a magnesium atom or Fe′, which does not. In Figure 24, we list these π-systems and the energy levels associated with them. The $\Delta H'_{xs}(y)$ for these "solid solutions" are readily evaluated and are shown in Figure 25 where the energy scale is in units of $-\beta$. Notice a strong dependence of the asymmetry on the electron count. Notice too that there is always an asymmetry toward the D_4 end-member, regardless of what the fractional π-electron count (n = 0.5, 1.0, or 1.5 electrons per π-orbital) may be. The dependence of the asymmetry on cluster stoichiometry (Figure 27) is very similar indeed to that found for both the solid solutions themselves (Figure 21) and the octahedral clusters used to model them. The electronic underpinnings of the asymmetry must lie in the orbital energies of Figure 24. It is easy to see that delocalization is directly responsible for such asymmetry. The energies of the levels of the $C_{4-y}D_y$ π-systems of Figure 24 do not depend linearly on the number of C–C–C interactions, and thus in the evaluation of the excess energy a residual will occur. The origin of the asymmetry is thus associated with the loss of long-range delocalization of orbitals as

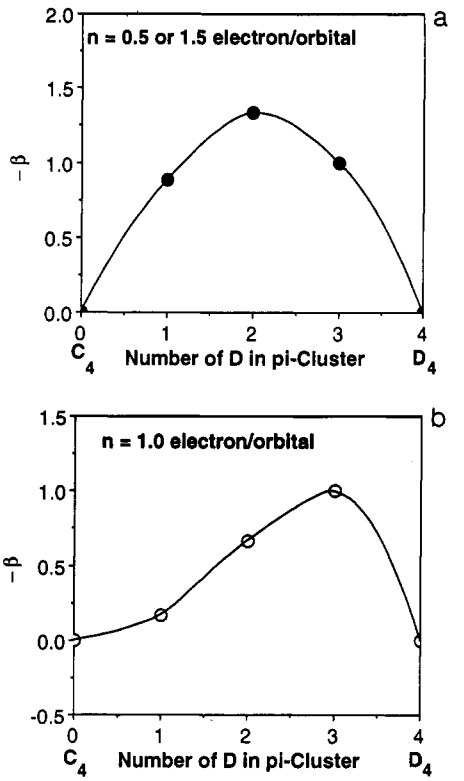

Figure 25. Total excess energy curves of $C_{4-y}D_y$ π-cluster solutions at three electron counts (n = 0.5, 1.0, and 1.5 electrons per π-orbital): (a) n = 0.5 or 1.5 electrons per π-orbital and (b) n = 1.0 electrons per π-orbital.

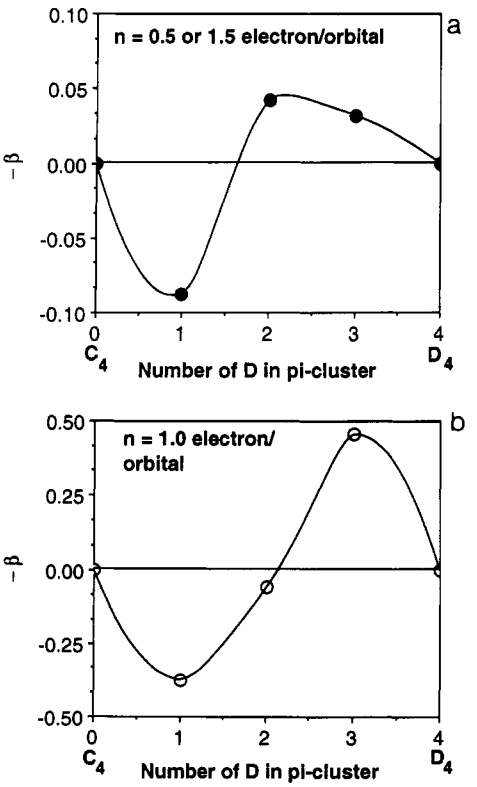

Figure 26. Residual excess energy curves of $C_{4-y}D_y$ π-cluster solutions at three electron counts (n = 0.5, 1.0, and 1.5 electrons per π-orbital): (a) n = 0.5 or 1.5 electrons per π-orbital and (b) n = 1.0 electron per π-orbital.

atoms are removed in the process C → D. By analogy for the oxide solid solutions it is the loss of metal d orbitals, Fe → Fe′ and M → Mg.

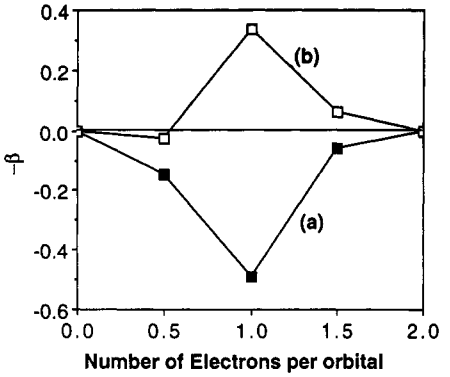

Figure 27. Residual excess energy curves of C_3D and CD_3 π-cluster solutions as a function of electron count.

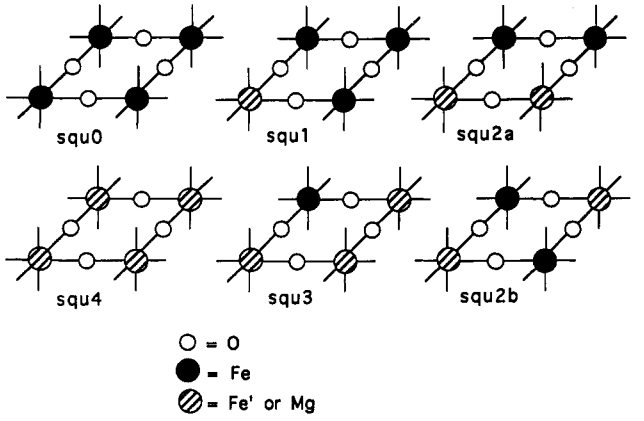

Figure 28. Square cluster solutions. The lines or sticks represent a metal–oxygen bonds as all the metals are octahedrally surrounded by oxygens.

Does this simple model carry over directly to the more complex metal oxide case? The answer is yes: a similar state of affairs holds in the series of square cluster solutions, $Fe_{4-y}Fe'_yO_{20}$ (Figure 28). Figure 29 shows the variation in $\Delta H'_{xs}(y)$ and in the residual energies with d count and composition. Figure 30 shows the calculated energy levels of the two sets of d orbitals, xy, and x^2-y^2, of π and σ type, respectively, which can take part in delocalized bonding in the square. These are exactly analogous to the π energy levels associated with the $C_{4-y}D_y$ π-systems of Figure 24. The energy level spectrum is qualitatively very similar in both cases and the origin of the asymmetry in the ΔH_{xs} plots has the same origin.

Local Distortions

Up until now we have modeled the solid solution problem by uniformly contracting or expanding the lattice dimensions while keeping the fractional atomic positions fixed. Since insertion of a guest A ion into a BO host of different size will in general lead to a local distortion, we have performed a series of calculations, similar to those described exhaustively above where oxygen atoms are displaced from their sites to preserve the A–O distance appropriate for that metal ion. In fact the set of $A_{B-y}B_yO_8$ solid solutions which we have chosen allow only a few specific ways by which the oxygens can be consistently moved from their general positions. For example, some solid solutions such as 2a, 4a, and 6a (Figure 2) have chains of AO and BO along the z axis. This highly symmetrical arrangement leads to no out-of-plane movement of the centered oxygen in the octahedral cluster. Figure 31 shows

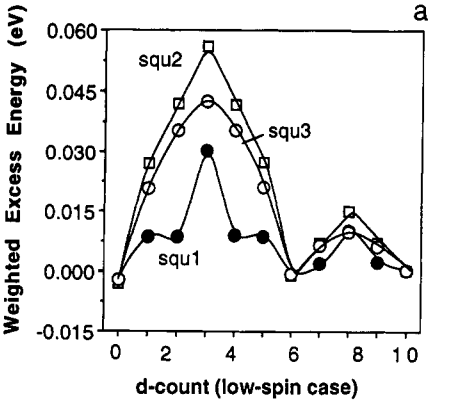

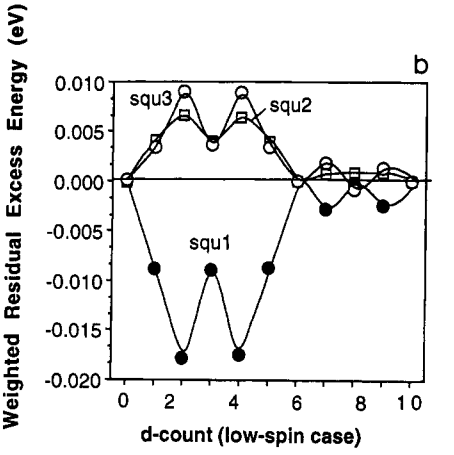

Figure 29. Low-spin weighted excess energies of square cluster solutions before and after the parabolic fit. (a) Before the parabolic fit, these energy distributions are the weighted total excess energies. (b) After the parabolic fit, they are weighted residual excess energies.

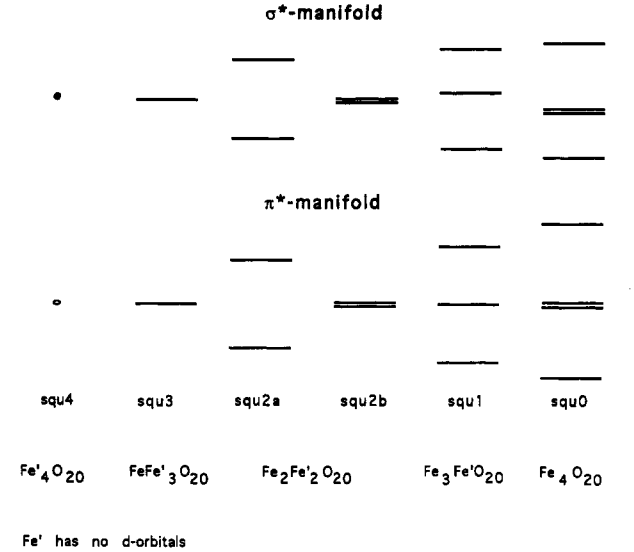

Figure 30. Selected molecular orbital diagrams of the $Fe_{4-y}Fe'_yO_{20}$ square cluster solutions. From left to right are the cluster solutions Fe_4O_{20} to Fe'_yO_{20}, with their respective MO diagram, solution type, and formula.

calculated results for the 27 solid solutions using the uniform and local distortion models for the (Fe,Mg)O solutions. The results are quite similar for the two cases, there being a somewhat larger spread of energies for a given composition in the distorted case. Figure 32 shows the contribution to $\Delta H'_{xs}(y)$ from the metallic substitution process. Again the spread is larger for the locally distorted

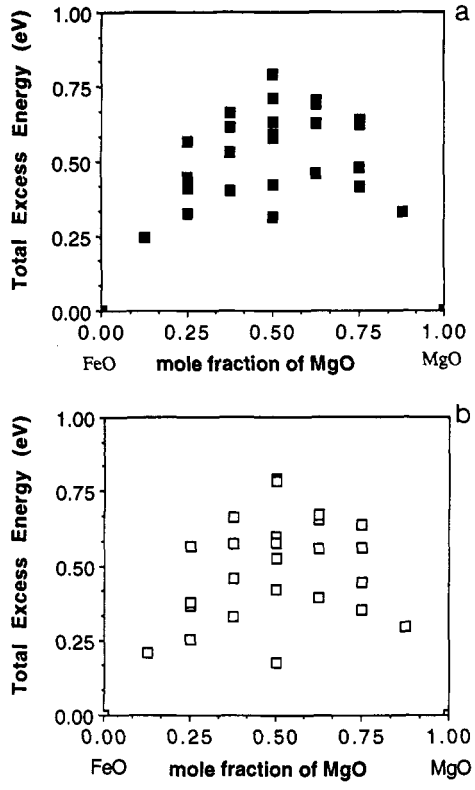

Figure 31. The 27 computed excess energies of regular and distorted (Fe,Mg)O solid solutions. In both (a) regular and (b) distorted (Fe,Mg)O solid solutions, the splitting or spread of excess energy values at a specific mole fraction of MgO are illustrated.

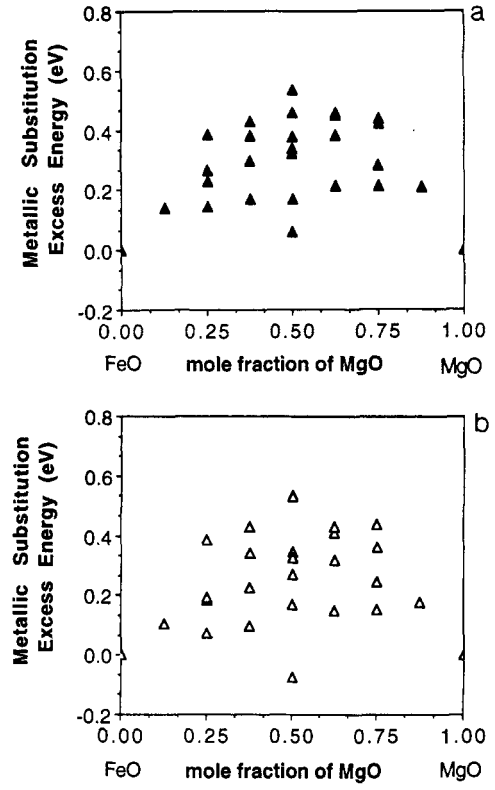

Figure 32. Metallic substitution excess energies of 27 regular and distorted (Fe,Mg)O solid solutions. In both (a) regular and (b) distorted (Fe,Mg)O solid solutions, the splitting or spread of excess energy values at a specific mole fraction of MgO are illustrated.

model and one point has become negative. There is a small effect of the local distortion on the residual energies. Our conclusion is that the overall picture is similar to that for the undistorted solutions. However, if a strong stabilization occurs for one member of the permutational set then perhaps ordering of the A, B, ions will occur.

Conclusions

We have been able to successfully decompose the calculated $\Delta H'_{xs}(y)$ plots into three parts, a two-atom term (identified with the volume change of solution formation), a three-atom term (identified with the bulk of the metallic substitution process and understandable in terms of the regular solution model), and an asymmetry term (due to the interruption of a delocalized network). The electron count dependence of the three terms enables an understanding of the reversal in the sign of $\Delta H_{xs}(x)$ on going from (Fe,Mg)O to (Ni,Mg)O. This decomposition is one which is similar to that often used successfully in the treatment of metallic solutions.[1c] We could regard our decomposition as being one which expressed the total energy in terms of many-atom potentials of various orders. Such models have recently come under particular scrutiny.[39,40] Particularly interesting in our case is that the energy seems to be quite well-converged for some of the d counts by the time the three-atom terms in ΔH_{MS} are included. For others the residual is significant and may well be accommodated by using a four-atom term as in the model of Figure 24.

It is important at this stage to ask how reliable our one-electron calculations are in modeling this behavior. Such computations are often not very good at reproducing energy changes associated with changes in bond length or volume but are usually a good way to study the energetics associated with "topological" problems, and especially how they change with electron count. Thus, of the three effcts we have mentioned, our conclusions concerning the last two are probably the most reliable. Particularly interesting is the failure of a mechanical model to reproduce the negative $\Delta H_{xs}(x)$ found for (Ni,Mg)O. It is clear that the nonelectrostatic part of this potential is ill-suited to view all three parts of the problem. Finally, ideas such as these should be applicable to other solid solutions especially the more complex oxides typical of the mineralogical world.

Acknowledgment. This research has been supported by the National Science Foundation (NSF DMR8819860). We would like to thank Drs. R. C. Newton, D. Heinz, and A. Navrotsky for several useful conversations.

(40) *Many-Atom Interactions in Solids*; Nieminen, R., Puska, M. J., Manninen, M., Eds.; Springer-Verlag: Berlin, 1990.